

ARTICLE

Received 29 Apr 2013 | Accepted 16 Oct 2013 | Published 15 Nov 2013

DOI: 10.1038/ncomms3779

OPEN

Arabidopsis SABRE and CLASP interact to stabilize cell division plane orientation and planar polarity

Stefano Pietra¹, Anna Gustavsson¹, Christian Kiefer¹, Lothar Kalmbach^{1,†}, Per Hörstedt², Yoshihisa Ikeda^{1,†}, Anna N. Stepanova³, Jose M. Alonso³ & Markus Grebe¹

The orientation of cell division and the coordination of cell polarity within the plane of the tissue layer (planar polarity) contribute to shape diverse multicellular organisms. The root of *Arabidopsis thaliana* displays regularly oriented cell divisions, cell elongation and planar polarity providing a plant model system to study these processes. Here we report that the SABRE protein, which shares similarity with proteins of unknown function throughout eukaryotes, has important roles in orienting cell division and planar polarity. SABRE localizes at the plasma membrane, endomembranes, mitotic spindle and cell plate. SABRE stabilizes the orientation of CLASP-labelled preprophase band microtubules predicting the cell division plane, and of cortical microtubules driving cell elongation. During planar polarity establishment, *sabre* is epistatic to *clasp* at directing polar membrane domains of Rho-of-plant GTPases. Our findings mechanistically link SABRE to CLASP-dependent microtubule organization, shedding new light on the function of SABRE-related proteins in eukaryotes.

¹Umeå Plant Science Centre, Department of Plant Physiology, Umeå University, SE-90 187 Umeå, Sweden. ²Umeå Core Facility Electron Microscopy, Umeå University, SE-90 187 Umeå, Sweden. ³Department of Genetics, North Carolina State University, Raleigh, North Carolina 27695, USA. † Present addresses: Department of Plant Molecular Biology, University of Lausanne, UNIL-Sorge, Biophore Building, 1015 Lausanne, Switzerland (L.K.); Centre of the Region Haná for Biotechnological and Agricultural Research, Department of Molecular Biology, Faculty of Science, Palacký University Olomouc, Šlechtitelů 11, 78371 Olomouc, Czech Republic (Y.I.). Correspondence and requests for materials should be addressed to M.G. (email: markus.grebe@umu.se).

Diverse multicellular organisms coordinate the polarity of single cells within the plane of the tissue layer^{1–5}. This type of tissue polarity is commonly referred to as planar polarity^{1,2,4}. The establishment of planar polarity is intensively studied for animal epithelia where *Drosophila* wing-hair polarization provides an invaluable model system^{1,2}. Similarly, plants like *Arabidopsis* display planar polarity of coordinated polar hair outgrowth from root epidermal cells^{3,4} and orientation of leaf epidermal hairs (trichomes)⁵. The upstream molecular mechanisms that direct planar polarity, however, differ substantially between animals and plants. In *Drosophila*, Wingless and its homologue dWnt4 act as long-range polarizing cues upstream of the Frizzled planar cell polarity pathway⁶, which transmits directional information to downstream effectors such as small Rho/Rac-type family GTPases^{1,2}. By contrast, plants lack genes with similarity to Wnts or to core components of the Frizzled planar cell polarity pathway. Instead, planar polarity of root epidermal cells is coordinated by a tissue concentration gradient of the plant hormone auxin^{4,7}. This gradient instructs the coordinated polar placement of hairs and of Rho-of-plant (ROP) GTPases that mark the initiation of planar polarity of root hair positioning before morphological hair outgrowth^{4,7}. ROP2/4 localization provides the earliest read-out for polar hair initiation^{8,9} and regulation of ROP activity spatially restricts polar root hair initiation^{9,10}. During morphogenesis of leaf pavement cells, auxin can activate ROP2/4 and ROP6 to differentially organize the actin and tubulin cytoskeleton, respectively^{11,12}. Actin and tubulin are also required for planar polarity of root hair initiation^{13,14}, but cytoskeletal dynamics and their regulation remain uncharacterized during this process. Similarly, the sole microtubule-associated protein known to be required for planar orientation of leaf trichomes is the CLIP170-associated protein (CLASP) from *Arabidopsis*¹⁵. Further, CLASP mediates orientation of cell division planes in roots^{16,17}, modulates the abundance^{18,19} as well as the polarity of PIN2 protein in root cortical cells¹⁹, and CLASP homologues regulate cellular asymmetries in other eukaryotes²⁰. At the molecular level, CLASP homologues associate with and stabilize the plus ends of dynamic microtubules²⁰, stabilize microtubule arrays during cell division^{15,16,20} and promote microtubule growth around cell edges contributing to the generation of plant cortical microtubule arrays²¹.

Here we report new functions for the *Arabidopsis* *SABRE* (*SAB*) gene, mechanistically linking its action to CLASP-mediated microtubule organization. We thus unravel new interactions contributing to the framework of cell division plane orientation and planar polarity formation in plants. Our findings may help to elucidate the function of uncharacterized *SAB*-like proteins found throughout eukaryotes and their potential function in cytoskeletal organization during cell division, cell morphogenesis and its coordination.

Results

***kreuz und quer* affects cell and planar polarity.** The root hairs of *Arabidopsis* regularly emerge from the outer membrane of epidermal cells and coordinately initiate close to, albeit not completely at, the root tip-oriented (basal) ends of cells (Fig. 1a). As knowledge about genes contributing to planar polarity in plants remains limited, we performed a genetic screen for root hair-positioning mutants to identify additional factors. This led to the identification of the recessive *kreuz und quer* (*kuq*) mutant generated by fast neutron mutagenesis. *kuq* displayed a more random distribution of hair position towards both the basal and the apical ends of cells (Fig. 1b,c). We also observed the localization of polar ROP protein patches at the outer membrane of root hair cells

before morphological hair outgrowth. Unlike wild type (Fig. 1d), *kuq* mutant cells often showed more basal or apical localization of ROP (Fig. 1e–g). In contrast, the polar distribution of PEN3-GFP (Supplementary Fig. S1a,b) that broadly defines the outer membrane^{22,23} as well as the apical polarity of the PIN2 auxin efflux carrier (Supplementary Fig. S1c,d) remained largely unaffected in root epidermal cells of *kuq* (Supplementary Fig. S1b,d). More strikingly, the polarity of GFP-BASL²⁴, which almost invariably localizes to basal membranes and to nuclei when ectopically expressed in wild-type root epidermal cells (99.8% basal, 0.2% of cells apical localization; $n = 514$) was significantly more often switched to apical ends of epidermal cells in *kuq* (8.6% of cells with apical localization; $n = 187$; $P = 5.1 \times 10^{-9}$ by Fisher's exact test; Supplementary Fig. S1e, f). These findings suggest that *kuq* affects basal membrane polarity and basal bias of planar polarity rather than outer lateral membrane polarity in the root epidermis.

Leaf trichome orientation provides another model for the analysis of both cell and planar polarity. *Arabidopsis* wild-type trichomes predominantly carry three branches, and the first branch, initiating closest to the leaf surface, is oriented towards the proximal end of the leaf^{5,15} providing a planar polarity read-out. Intriguingly, orientation of the first branch proved much more variable in the *kuq* mutant than in the wild type (Fig. 1h–j), revealing defective planar polarity of trichome orientation. At the cellular level, *kuq* mutant leaves showed two-branched trichomes more often than wild-type leaves (Fig. 1k,l; for quantitative analysis see below) and sometimes displayed irregular placement of branches along the trichome stalk (Fig. 1m). The reduction in branch number and the ectopic placement of branches on trichomes in *kuq* indicated a cell polarity defect in the initiation and placement of trichome branches. Interestingly, reduced trichome branch number has been reported for *Arabidopsis* mutants defective in tubulin and microtubule-associated proteins²⁵. Hence, *kuq* affects cell and planar polarity in leaf and root epidermis, causing phenotypes characteristic of microtubule cytoskeleton mutants.

***kuq* is allelic to *SABRE*.** We mapped the *kuq* mutation to a 480-kb interval on chromosome 1 by positional cloning (Fig. 2) and analysed phenotypes of T-DNA insertion lines in candidate genes within this interval. Homozygous seedlings from 9 out of 11 T-DNA insertion lines in one of these genes, *SABRE* (*SAB*) (At1g58250; Fig. 2) displayed phenotypes indistinguishable from that of *kuq*, whereas two showed similar but weaker seedling root and adult shoot defects (Figs 2 and 3a). Sequencing of the genomic *SAB* coding region in *kuq* identified a single-nucleotide deletion at position 6,592 (of 7,824), predicted to induce a non-sense mutation generating a premature stop codon (Fig. 2). Other *SAB*-mutant alleles have been described to display anisotropic expansion of root cortical cells^{26–28} or an enhanced response to phosphate starvation²⁹. More detailed analysis of three *SAB* T-DNA insertion lines, SALK 108709 (*sab-5*), SALK 52995 (*sab-6*) and SALK 123771 (*sab-7*) uncovered reduced epidermal cell length and defective planar polarity of root-hair position similar to that of the *kuq* mutant (Fig. 3b–e). Complementation analyses revealed that these three lines were allelic to *kuq* and to each other and they are, therefore, in the following referred to as *sab^{kuq}*, *sab-5*, *sab-6* and *sab-7*. The *sab-7* mutant carrying an insertion into the second last exon of the *SAB* gene (Fig. 2) was somewhat less affected, identifying it as a hypomorphic allele (Fig. 3a,b,e). Reverse transcription PCR (RT-PCR) analyses revealed that neither *sab-5*, *sab-6* nor *sab-8* (SALK 12897) produced a full-length transcript, in contrast to *sab^{kuq}* for which a transcript could be detected when using primers spanning the

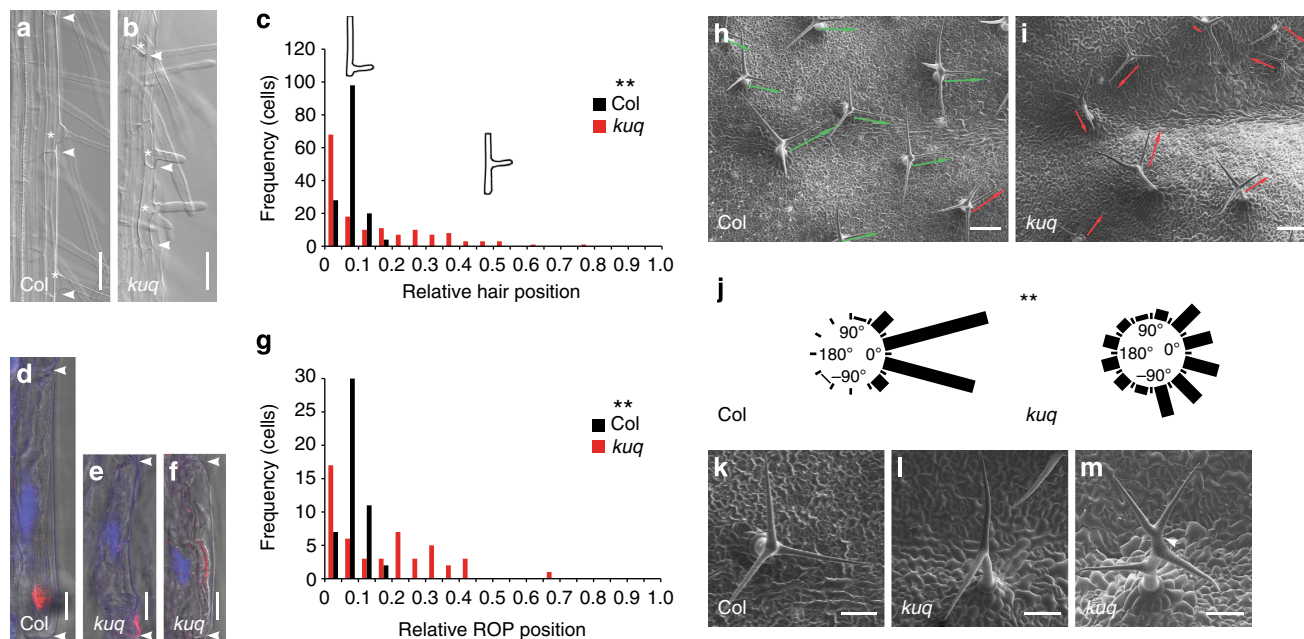


Figure 1 | *kuq* mutation affects epidermal cell and planar polarity. (a,b) Hair-forming root epidermal cells of 5-day-old (a) wild-type Columbia (Col) and (b) *kuq* seedlings. Arrowheads, apical and basal ends of cells in a, b and d-f. Asterisks indicate sites of hair formation in a and b. (c) Quantitative analysis of planar polarity phenotypes as relative root hair position in Col and *kuq*. Number of cells in classes (frequency) with hair positions are indicated between basal (0) and apical (1) ends of cells (** $P=0.000$ Col versus *kuq*, determined by non-parametric, two-sample Kolmogorov-Smirnov (K-S) test, $n=150$ cells from 30 roots per genotype). (d-f) anti-ROP (red) immunofluorescence in Col, (e,f) *kuq* epidermal cells, combined with DAPI-stained nuclei (blue) and brightfield microscopy image. (g) Quantitative analysis of planar polarity phenotypes of ROP protein patch positions along apical-basal axis of epidermal cells in Col and *kuq*. Number of cells in classes (frequency) showing ROP positions between basal (0) and apical (1) ends is shown (** $P=0.000$ Col versus *kuq* by K-S test, $n=50$ cells per genotype, from 10 Col and 19 *kuq* roots). (h,i,k-m) Scanning electron microscopy (SEM) images of leaf trichomes of (h,k) Col, (i,l,m) *kuq*-mutant leaves. (h,i) Planar polarity of first trichome branch orientation along proximo-distal leaf axis (arrows). Distal ends of leaves are to the left, proximal ends to the right. Deviation of $<30^\circ$ and $>30^\circ$ from proximal orientation is indicated by green and red arrows, respectively. (j) Quantitative analysis of first trichome branch orientation from SEM images of Col and *kuq*. 0° indicates proximal orientation, 180° distal orientation of trichome branches. (** $P<0.001$ Col versus *kuq* by F-test, $n=174$ trichomes per genotype). (k-m) Trichome branching phenotypes of (k) Col and (l,m) *kuq*. Note, (l) trichomes with two branches or (m) additional ectopically placed branch in *kuq* (arrowhead). For statistical analysis, see Fig. 5a. Scale bars, $50\ \mu\text{m}$ (a,b), $10\ \mu\text{m}$ (d-f), $200\ \mu\text{m}$ (h,i), $100\ \mu\text{m}$ (k-m).

region including the single-nucleotide deletion (Fig. 3f-h). We subsequently employed *sab-5* in parallel to or instead of *sab^{kuq}* because *sab-5* carried the T-DNA insertion closest to the 5'-end of the *SAB* coding region (Fig. 2), did not express full-length *SAB* complementary DNA (cDNA) (Fig. 3f-h) and displayed phenotypic defects similar to *sab^{kuq}* (Fig. 3a-c, Supplementary Fig. S2a-l). Thus, cloning of *sab^{kuq}* revealed a central role for *SAB* in cell and planar polarity.

SABRE-like proteins in other eukaryotes. Our sequencing of *SAB* wild-type cDNA amplified from *Arabidopsis* roots experimentally verified the presence of an 8,347-bp transcript encoding a 2,607 amino acid protein identical to the predicted protein sequence At1g58250.1 (ref. 29). Depending on the transmembrane helix prediction algorithm employed, *SAB* is predicted to contain one (TMHMM, Pred-TMR), two (TMpred) or three transmembrane domains (TopPred2, HMMTOP). All programs predict the first six to eight amino-terminal amino acids preceding the first transmembrane domain to be cytosolic. This indicates that *SAB* contains an internal, hydrophobic start-transfer sequence rather than an N-terminal cleavable signal peptide and that *SAB* may be a transmembrane protein rather than a secreted protein. Proteins with sequences related to the predicted 2,607 amino acid *SAB* protein are found throughout diverse eukaryotes (Fig. 4a). In *Arabidopsis thaliana*, KINKY

POLLEN (KIP) shares the highest sequence identity with *SABRE*²⁸. Although plant species harbour either one or two *SAB*-like genes in their genomes, all animal genomes analysed, including the human and mouse genomes, possess a single-copy gene encoding a protein of similar size with highest sequence identity restricted to two larger protein regions (Fig. 4b). To date, none of the genes related to *SAB* from non-plant eukaryotes has been functionally characterized. However, mutants defective in the *Arabidopsis KIP* gene and the closely related *ABERRANT POLLEN TRANSMISSION1 (APT1)* gene from maize are defective in pollen tube growth^{28,30}. *APT1*, like *SAB*, codes for a predicted 2,607 amino acid protein³⁰. When transiently expressed in tobacco pollen, a carboxy-terminal 108 amino acid peptide from *APT1* fused to green fluorescent protein (GFP) localizes to the Golgi apparatus³⁰. The peptide has been annotated as a Golgi-body localization domain in the conserved domain database³¹. However, although *SAB* is a predicted membrane protein with the N terminus oriented towards the cytosol, the biological and molecular function of *SAB* and related proteins as well as the subcellular localization of full-length proteins remain to be addressed in any eukaryote.

SAB-CLASP interaction in planar polarity. As the *SAB* sequence did not provide information about the molecular function of the protein, we addressed the mechanism of *SAB*

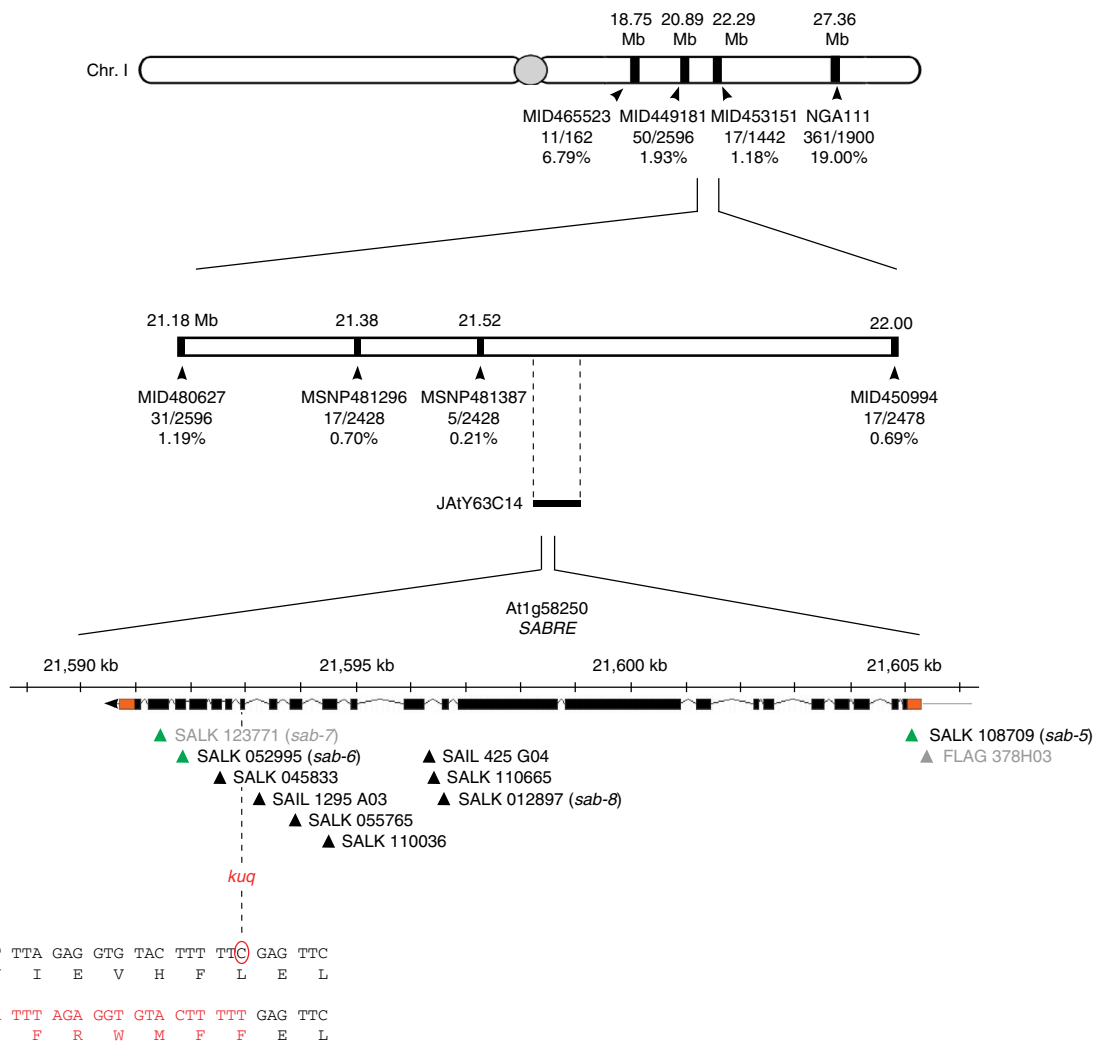


Figure 2 | *kuq* causes a single-nucleotide deletion in the *SABRE* gene. Map-based identification of the *kuq* mutation in the *SAB* gene. Simple-sequence-length polymorphism (SSLP; NGA111), custom-made SSLPs (Monsanto Insertion/Deletion polymorphism; MID) and custom-made cleaved amplified polymorphic sequence (CAPS; MSNP) markers are indicated with respective position, recombinant/total chromosomes and recombination frequency. Digits of MID and MSNP markers correspond to polymorphism accession number in Monsanto *Arabidopsis* Polymorphism Collection (<http://www.arabidopsis.org/browse/Cereon/index.jsp>). Note the 480-kb mapping interval containing JAtY63C14 transformation-competent bacterial artificial chromosome carrying the *SAB* gene. Insertion positions of 11 *SAB* T-DNA lines analysed are indicated by arrowheads below the gene structure. Black boxes, exons; lines, introns; orange boxes, untranslated regions. T-DNA lines in black, homozygous seedlings phenotypically indistinguishable from *kuq* mutants; T-DNA lines in grey, weaker phenotype. T-DNA lines with green arrowheads, tested for allelism to *kuq* by complementation test. Red circle, cytosine deletion in *kuq* inducing a premature stop codon in 17th exon of *SAB*; upper rows, wild-type coding sequence and amino-acid translation; lower rows, *kuq*.

action by analysing its genetic interactions. The combination of trichome branching and orientation defects observed in *sab* mutants had been described for *clasp* mutants¹⁵. We therefore generated a *sab-5;clasp-1* double mutant and observed a strongly enhanced trichome branching defect, when compared with the respective single mutants or *sab^{kuq}* (Fig. 5a; Supplementary Fig. S3a,b), suggesting that *SAB* and *CLASP* synergistically interact during placement of trichome branches. Similarly, root length and overall growth of *sab-5;clasp-1* double-mutant seedlings was severely reduced compared with the single mutants, further pointing towards a synergistic interaction at this level (Fig. 5b; Supplementary Fig. S3c).

We next addressed whether *CLASP* acts on planar polarity of root hair placement and observed a clear basal shift of hair position in *clasp*-mutant alleles (Fig. 5c–e). Similarly, ROP protein patches were misplaced towards the basal-most ends of elongating *clasp*-mutant epidermal cells when compared with the

wild type (Fig. 5f–h), demonstrating that *CLASP* acts on planar polarity before ROP positioning. Strikingly, ROP positioning in *sab-5;clasp-1* double-mutant seedlings was indistinguishable from that of *sab-5* (Fig. 5i–k), suggesting that *sab* is epistatic to *clasp* during polar ROP positioning.

***SAB-CLASP* interaction during division plane orientation.** The genetic interactions between *SAB* and *CLASP* prompted us to investigate whether *SAB* contributes to other processes that involve *CLASP* function, such as orientation of the cell division plane. Strikingly, *sab-5*- and *sab^{kuq}*-mutant root meristems displayed strongly aberrantly orientated cell division planes when compared with the wild type (Fig. 6a,b; Supplementary Fig. S3d,e). Live imaging of microtubules and nuclear DNA co-visualized by mCherry-TUBULIN ALPHA-5 (mCherry-TUA5)^{32,33} and HISTONE2B-YELLOW FLUORESCENT

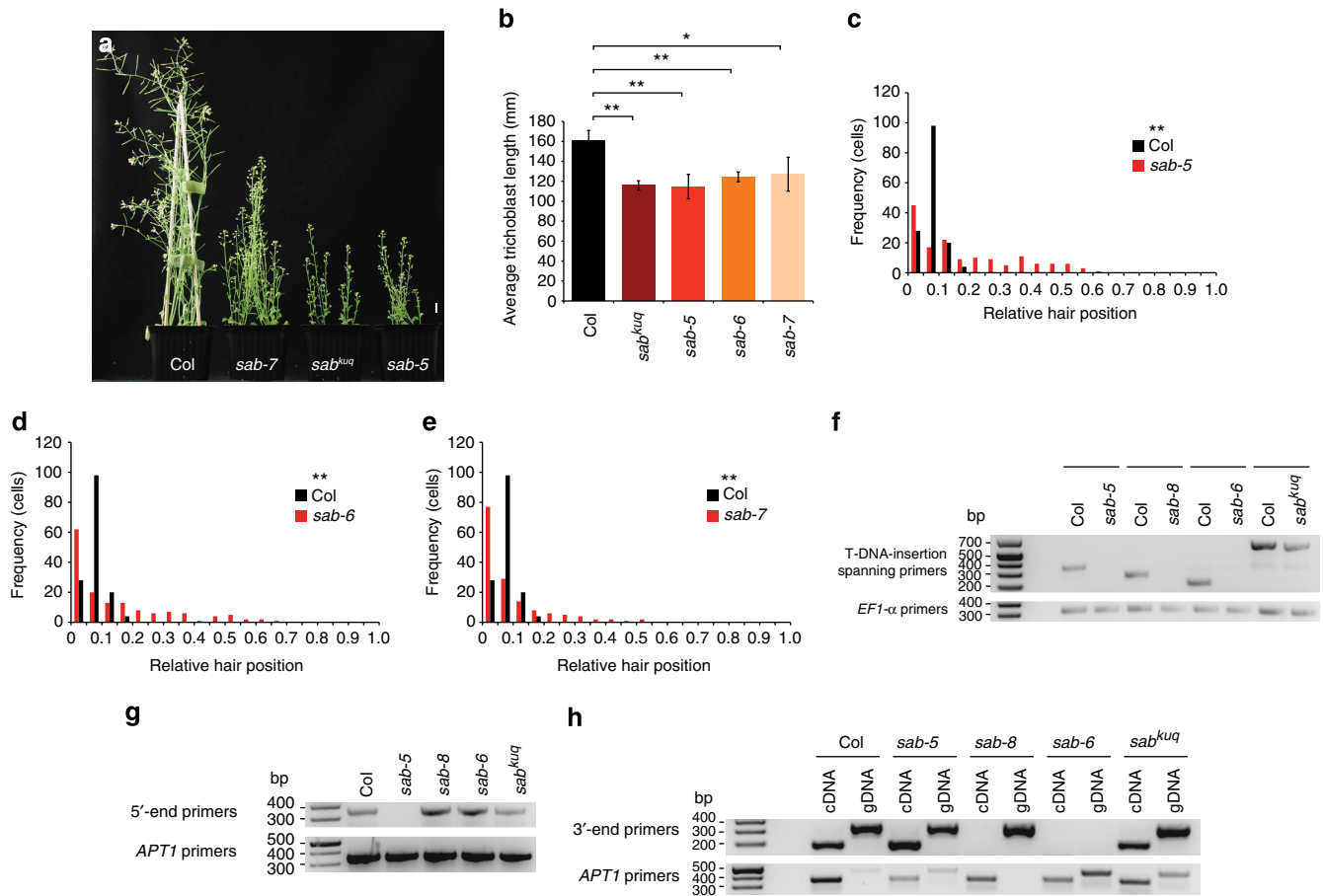


Figure 3 | Phenotypic and RT-PCR analyses of additional SAB T-DNA-mutant alleles. (a) Five-week-old plants of Col, *sab-7*, *sab^{kuq}* and *sab-5*. Note, *sab-5* is indistinguishable from *sab^{kuq}* while *sab-7* is less affected. (b) Quantitative analysis of trichoblast length in Col and SAB-mutant alleles. Average cell length of *n* = 150 trichoblasts from 30 roots per genotype. Data are means ± s.d. from *n* = 3 independent experiments. Statistical differences determined by two-tailed, unpaired *t*-test with equal variance and significance level *P* < 0.05 are indicated as **P* < 0.05 and ***P* < 0.01; *n* = 3. All *sab* alleles differ significantly from wild type but do not differ from each other (*P* > 0.05). (c–e) Quantitative analysis of planar polarity defects in (c) *sab-5*, (d) *sab-6* and (e) *sab-7* compared with Col is displayed as relative root hair position similar to Fig. 1c. ***P* = 0.000 Col versus *sab-5*, *sab-6* or *sab-7* by K-S test, *n* = 150 cells from 30 roots per genotype. (f–h) Semiquantitative RT-PCR analysis of wild-type Col and *sab*-mutant seedlings. SAB transcript was amplified with (f) primers spanning the T-DNA insertion (or single-nucleotide deletion) and primers located close to (g) the 5'- or (h) the 3'-end of SAB coding sequence. Primers close to 3'-end were also employed on genomic DNA (gDNA) extracted from the same plant material used for cDNA (cDNA) synthesis. Partial SAB transcripts were detected in all T-DNA alleles. *EF1-α* and *APT1* were utilized as controls. Scale bar, 10 mm.

PROTEIN (H2B-YFP)³⁴, respectively, revealed that in comparison with wild type (Fig. 6c), *sab-5*-mutant cells displayed misorientation of the preprophase band (PPB; Fig. 6d). This orientation defect was followed by similarly misaligned spindle and phragmoplast orientation throughout mitosis and cytokinesis, whereas the overall timing of mitosis and cytokinesis was indistinguishable from wild-type root cells (Fig. 6d; Supplementary Movies 1 and 2). Similar results were obtained in immunolocalization studies demonstrating that PPB, spindle and phragmoplast orientation were defective in epidermal cells of both *sab-5*- and *sab^{kuq}*-mutant root meristems (Fig. 6e–q; Supplementary Fig. S3f–h). PPB, spindle and phragmoplast orientation in the *sab-5;clasp-1* double mutant did not statistically differ from the *sab-5* single mutant, but were significantly more strongly affected than in the *clasp-1* single mutant (Fig. 6o–q). Thus, SAB function is required for cell division plane orientation already before or at the level of PPB orientation and *sab* shows epistasis over *clasp* during this process. Further, in comparison with wild type (Fig. 6r), the orientation of functional GFP-CLASP²¹ on *sab-5* mutant PPBs was affected and coincided with the misoriented alignment of PPB microtubules

(Fig. 6s,t). These results suggested that SAB function is required for orientation of CLASP-guided cortical microtubules and stabilizes correct placement of PPB microtubules in the future plane of cell division.

SAB acts on cortical microtubule arrays. We next analysed potential effects of SAB on cortical microtubule orientation in late meristematic epidermal cells at the transition to cell elongation, in rapidly expanding cells, and during later stages of hair cell differentiation. Strikingly, in contrast to the transversal orientation of mCherry-TUA5-marked microtubules observed in both late meristematic cells (Supplementary Fig. S4a) and in rapidly elongating wild-type cells (Fig. 7a), *sab-5*-mutant cells of the same size displayed a more random orientation of cortical microtubules than wild-type cells in both cases (Supplementary Fig. S4b,c; Fig. 7b,c). We further monitored the directionality of microtubule growth using the microtubule plus end-tracking protein (+ TIP) AtEB1a-GFP³⁵ in combination with mCherry-TUA5. This revealed bidirectional movement of transversally oriented cortical microtubules in elongating wild-type cells and of the

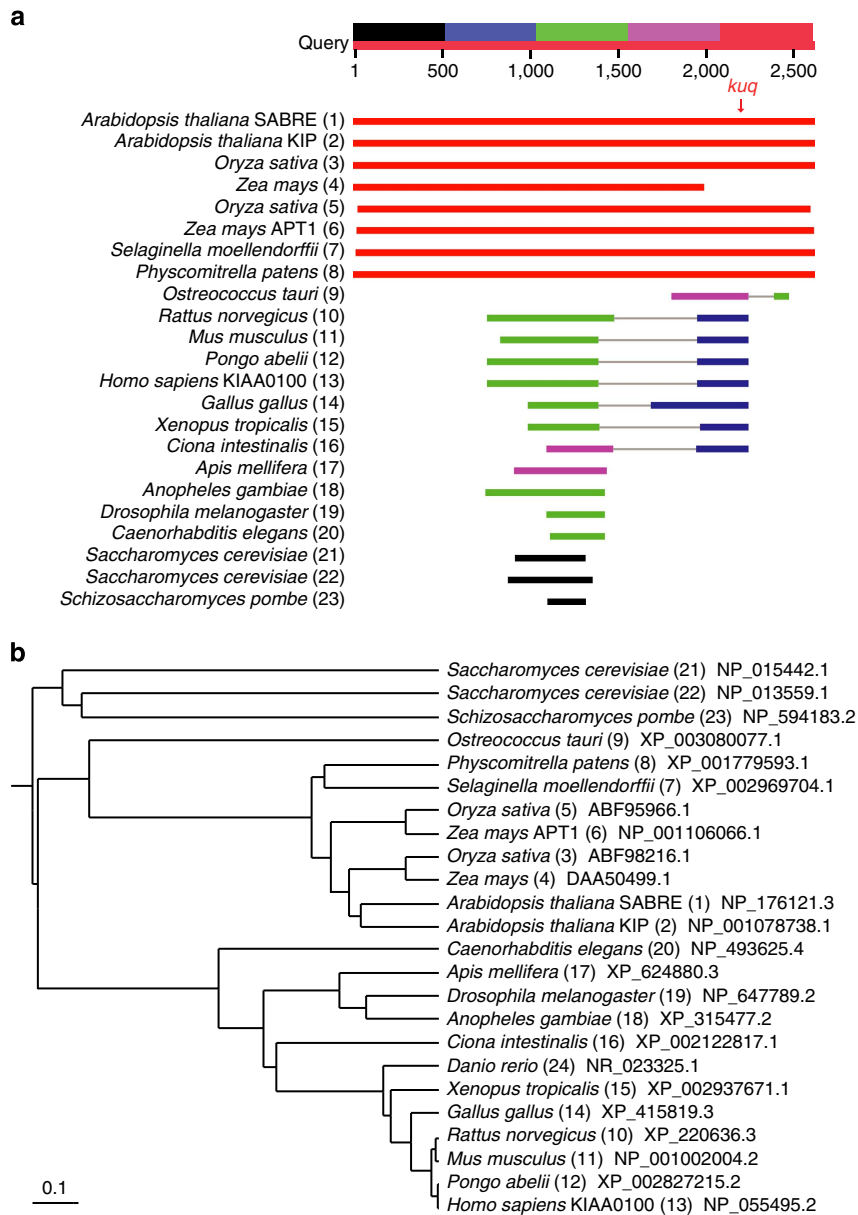


Figure 4 | SAB-related proteins in diverse eukaryotes. (a) Blastp search for proteins homologous to SAB and alignment of SAB-like protein sequences from selected organisms. Note, sequence similarity with proteins from more distantly related species is restricted to two distinct regions of about 600 and 300 amino acids. Red arrow, position of premature stop codon introduced by *kuq* mutation. Numbers in parentheses refer to sequences in **b**. Red, alignments with highest sequence identity; black, lowest sequence identity. (b) Phylogenetic tree based on sequences of SAB-related proteins in selected species, showing evolutionary conservation of SAB across a wide variety of eukaryotic organisms. NCBI reference sequence or GenBank accession number for each protein are indicated next to the respective species.

more randomly oriented microtubules in *sab-5*-mutant epidermal cells (Fig. 7a,b; Supplementary Movies 3 and 4). Intriguingly, elongating trichoblasts just before hair initiation displayed a reoriented, bipolar arrangement of longitudinally growing microtubules (Fig. 7d; Supplementary Movie 5), where the majority of microtubule plus ends grew with apical directionality at apical ends of cells (Fig. 7e) and with basal directionality at basal ends of cells (Fig. 7f). This bipolarity of microtubule growth resembled the one recently described for elongating hypocotyl cells³⁶. The overall longitudinal orientation and bipolarity of microtubule growth was less clearly axially aligned in *sab-5*-mutant cells (Fig. 7g; Supplementary Movie 6). In addition, mCherry-TUA5 co-visualized with the root hair initiation site marker PIP5K3-YFP³⁷ revealed an accumulation

of radially reorganized cortical microtubules at the root hair initiation site in 45% of the cells observed (32/71; Fig. 7h–l; Supplementary Fig. S4d,e), whereas 55% did not harbour such an array (Supplementary Fig. S4f,g). The majority of cells (94%, 67/71) at this differentiation stage showed longitudinally oriented microtubules interspersed in diffuse, cytosolic mCherry-TUA5 fluorescence indicative of microtubule depolymerization and reorganization in these cells (Fig. 7i; Supplementary Fig. S4d–g). In comparison, only a minority of cells (6%, 4/71) still revealed transversal microtubule orientation, when hair initiation sites were already marked by PIP5K3-YFP. Although we did occasionally observe reorganized cortical microtubules at PIP5K3-YFP-marked hair initiation sites in *sab-5*-mutant cells (Fig. 7m–o), none of these cells (0%, 0/50) displayed one unique

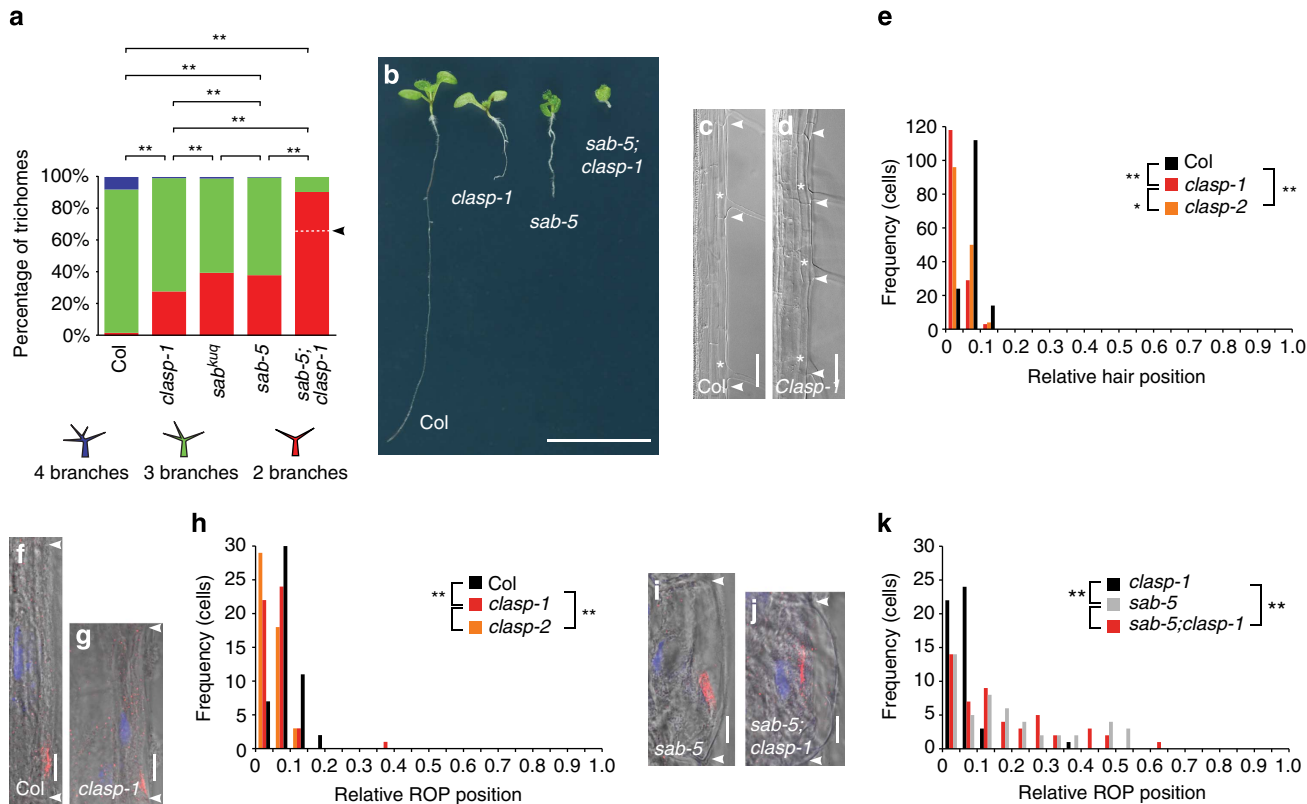
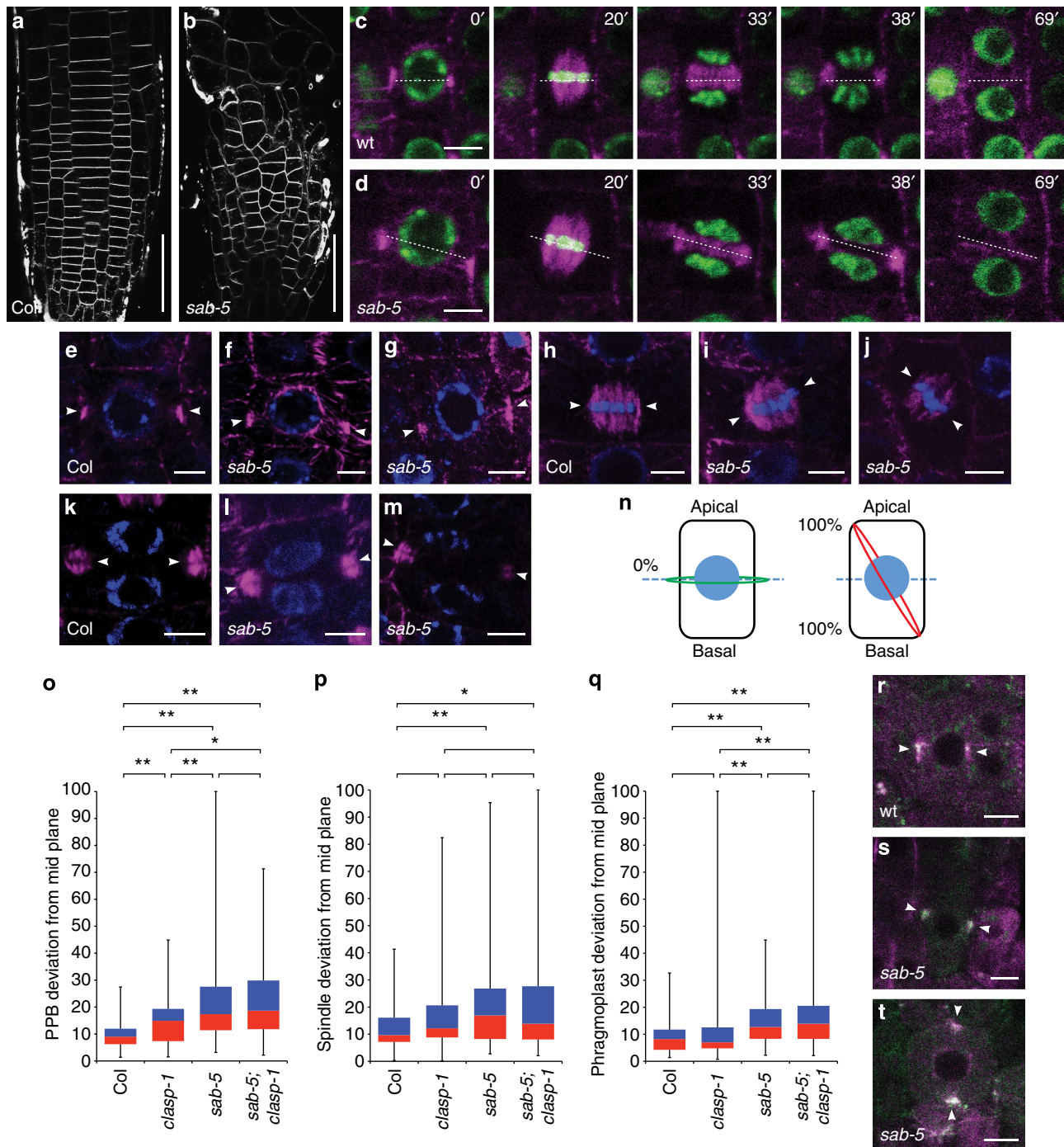


Figure 5 | SAB-CLASP interaction mediates planar polarity upstream of ROP. (a–k) Genetic action of *sab* and interaction with *clasp* during (a) leaf trichome branching, (b) seedling development and (c–k) planar root epidermal polarity establishment. (a) Percentage of 2-branched (red), 3-branched (green) and 4-branched (blue) trichomes in Col (total trichome number: $n = 545$), *clasp-1* ($n = 537$), *kuq*-mutant allele of *SAB* (*sab^{kuq}*; $n = 409$), *sab-5* ($n = 498$) and *sab-5; clasp-1* ($n = 431$) obtained from 10–16 leaves per genotype. Note, significant differences between all genotypes except for *sab-5* and *sab^{kuq}* ($P = 0.51$); the percentage of 2-branched trichomes in *sab-5; clasp-1* highly significantly differed from the sum of the respective single-mutant values (dotted line, arrowhead; $P < 0.001$). Significances were determined by Fisher’s exact test with significance level $P < 0.05$ and are indicated as $**P < 0.01$. Supplementary Table S1 shows exact P -values. (b) Ten-day-old Col, *clasp-1*, *sab-5* and *sab-5; clasp-1* seedlings. (c,d) Root hair position on epidermal cells of 5-day-old (c) Col and (d) *clasp-1* seedlings. (e) Quantitative analysis of planar polarity in Col, *clasp-1* and *clasp-2* is displayed as relative root hair position as in Fig. 1c. ($**P = 0.000$ Col versus *clasp-1*; $**P = 0.000$ Col versus *clasp-2* by K-S test; $n = 150$ cells per genotype). (f,g,i,j) Planar polarity phenotypes revealed by anti-ROP immunolabelling (red), DAPI (blue) overlaid with brightfield image of epidermal cells from (f) Col, (g) *clasp-1*, (i) *sab-5* and (j) *sab-5; clasp-1*. (h,k) Quantitative analysis of polar ROP protein patch positions as in Fig. 1g. (h) Col, *clasp-1*, *clasp-2*, (k) *clasp-1*, *sab-5* and *sab-5; clasp-1* ($**P = 0.004$ Col versus *clasp-1*; $**P = 0.000$ Col versus *clasp-2*; $P = 0.241$ *clasp-1* versus *clasp-2*; $**P = 0.000$ *clasp-1* versus *sab-5*; $**P = 0.000$ *clasp-1* versus *sab-5; clasp-1*; $P = 0.841$ *sab-5* versus *sab-5; clasp-1* by K-S test, $n = 50$ cells from 8 to 22 roots per genotype). Arrowheads, apical and basal ends of cells in c, d, f, g, i and j. Asterisks indicate sites of hair formation in c and d. Scale bars, 10 mm (b), 50 μm (c,d), 10 μm (f,g,i,j).

radial rearrangement that could be unambiguously identified as preceding a hair initiation site comparable to the situation in wild type (Fig. 7m–o; Supplementary Fig. S4h–k). Hence, because of the irregular cortical microtubule arrangement in *sab-5*, microtubule organization did not allow for prediction of the positions of hair initiation sites. However, PIP5K3-YFP-marked hair initiation sites occurred in ectopic basal-most, or more apical positions along *sab-5*-mutant hair cells (Fig. 7m–p; Supplementary Fig. S4h–k), when compared with the wild type (Fig. 7h–j,p; Supplementary Fig. S4d–g). These findings suggest that *SAB* activity is required for cortical microtubule reorganization at correct sites before hair outgrowth. Thus, *SAB* function mediates transversal microtubule alignment in elongating cells and polar placement of domains of reorganizing microtubules in cells initiating hair formation.

SAB subcellular localization. We next determined the subcellular localization of the predicted full-length 290 kDa *SAB* protein encoded by a messenger RNA of low abundance^{27,28}. To this end, we employed recombineering³⁸ to insert three

consecutive copies of the cDNA encoding for the bright fluorescent protein Ypet (3xYpet) at the 5′- or at the 3′-end of the genomic coding sequence of *SAB*. Both constructs rescued the overall *sab-5* growth defect and all phenotypes investigated, including cell division plane orientation and planar polarity of root hair initiation (Fig. 8a–g). The planar polarity phenotype of *sab-5* was fully rescued by *SAB*-3xYpet and largely, albeit not completely, by 3xYpet-*SAB* (Fig. 8f,g). Both constructs were expressed at low levels throughout the root tip and displayed indistinguishable subcellular distribution (Figs 8h–l and 9a,b). These results suggested a likely orientation of both the N- and the C-terminus towards the cytosol because fluorescence of cell wall-oriented GFP and YFP protein tags has been reported to be quenched by the low cell wall pH (refs 39,40). 3xYpet-*SAB* and *SAB*-3xYpet localized in patches at the cell periphery, suggesting localization to the plasma membrane or cell wall and to endomembrane compartments (Figs 8k,l and Fig. 9a,b). Plasmolysis experiments in the presence of a cell wall marker revealed retraction of *SAB*-3xYpet from the cell wall (Fig. 9c,d). Strikingly, meristematic cells showed clear enrichment of



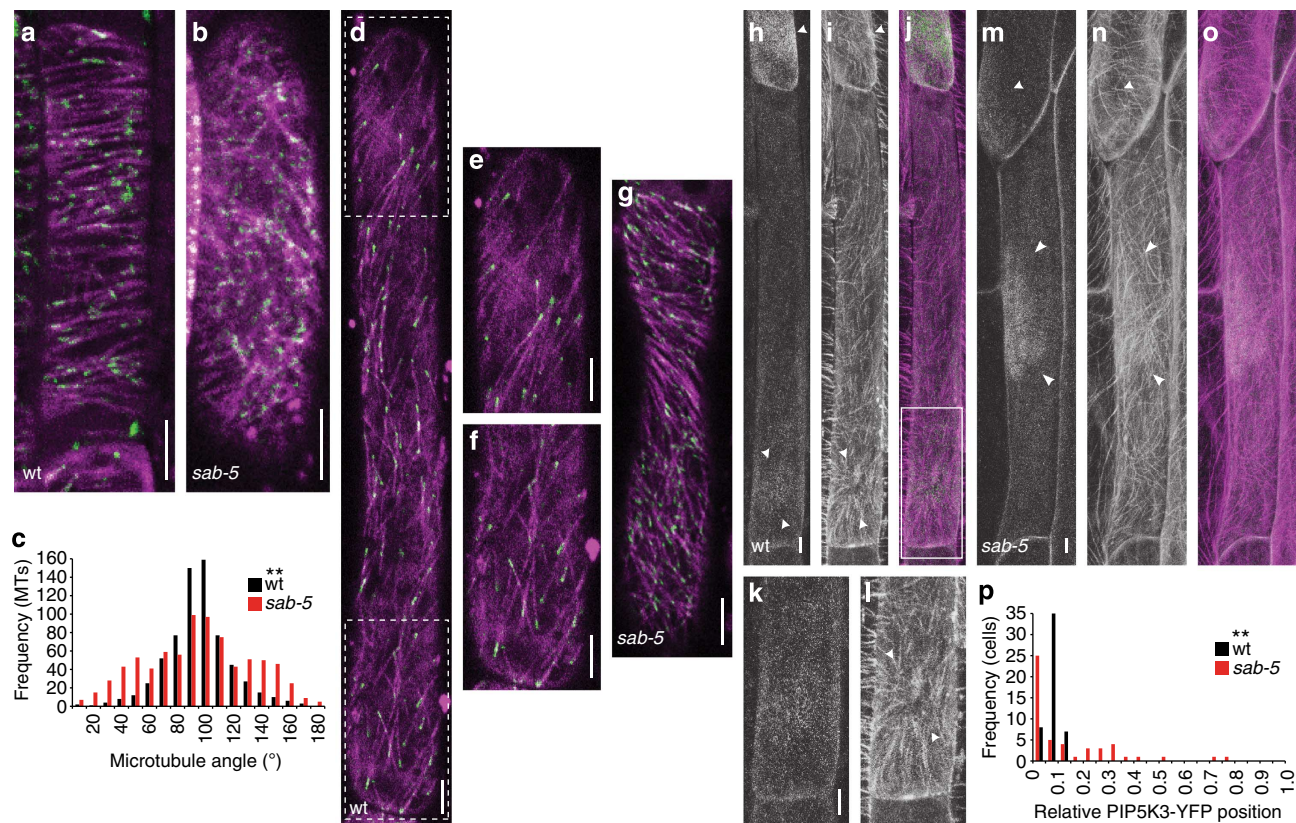


Figure 7 | SAB is required for cortical microtubule orientation during cell elongation and planar polarity. (a,b) Live imaging of cortical microtubule arrays in early elongation stage root hair cells co-expressing mCherry-TUA5 (magenta) and the plus end-tracking protein AtEB1a-GFP (green). Note, (a) transversal orientation in wild type (wt; *SAB/SAB* or *SAB/sab-5*), versus (b) more random orientation in *sab-5* homozygote (*sab-5*). (c) Quantitative analysis of microtubule angles relative to the apical-basal cell axis in hair cells of 26–36 μm length from phenotypically wt and *sab-5* seedlings. Statistical analysis reveals highly significant difference between wt and *sab-5* ($^{***}P=0.000$ by K-S test, $n=673$ microtubules analysed for wt and $n=802$ for *sab-5*, from 28 and 20 cells). For similar results on late meristematic cells of 13–18 μm length, see Supplementary Fig. S4a–c. (d–g) Live imaging of cortical microtubule arrays in later elongation stage root hair cells co-expressing mCherry-TUA5 (magenta) and the plus end-tracking protein AtEB1a-GFP (green). (d) Bipolar axial orientation of microtubule growth in wt cell just before first hair formation. (e,f) Magnifications of regions marked in d, showing plus ends of microtubules preferentially growing towards (e) apical and (f) basal ends of cell. (g) Perturbed axial alignment and growth of microtubules in *sab-5*-mutant cell. (h–o) Live co-imaging of mCherry-TUA5-labelled microtubules with hair initiation site marker PIP5K3-YFP. (h) PIP5K3-YFP, (i) mCherry-TUA5, (j) merge of PIP5K3-YFP (green) and mCherry-TUA5 (magenta) in wt cells. (k,l) Magnifications of inset in j, showing (k) PIP5K3-YFP and (l) mCherry-TUA5 at hair initiation site. (m) PIP5K3-YFP, (n) mCherry-TUA5, (o) merge of PIP5K3-YFP (green) and mCherry-TUA5 (magenta) in *sab-5*. Arrowheads, microtubule (re-)organization at (i) close-to-basal site in wt versus (n) basal-most or apically shifted sites in *sab-5*. (p) Quantitative analysis of polar PIP5K3-YFP patch position, marking site of root hair initiation. Number of cells in classes (frequency) showing PIP5K3-YFP position between basal (0) and apical (1) ends of epidermal cells is shown ($^{***}P=0.000$ wt versus *sab-5* by K-S test, $n=50$ cells per genotype from 39 wt and 41 *sab-5* roots). For additional microtubule visualization, see Supplementary Fig. S4d–k. Scale bars, 5 μm .

SAB-3xYpet at domains of apical and basal plasma membranes that had just started to retract from the cell wall at the onset of plasmolysis (Fig. 9c). Similarly, transversal, apical-basal membranes of non-plasmolysed cells showed an enrichment of SAB-3xYpet (Fig. 9a) and 3xYpet-SAB co-localization with the plasma membrane marker NSPN12-mCherry/WAVE131R (ref. 41; Fig. 9e). Co-visualization of SAB-3xYpet with endoplasmic reticulum (ER; Fig. 9f), Golgi (Fig. 9g) and *trans*-Golgi network (TGN) (Fig. 9h) markers^{41,42} revealed that the endomembrane compartments containing 3xYpet-SAB/SAB-3xYpet did neither represent ER, Golgi nor TGN (Fig. 9f–h). Our findings do not support the previously posed hypotheses that full-length SAB-like proteins may be Golgi-localized or secreted at steady state, respectively^{28,30}. Rather, our results provide *in vivo* evidence corroborating the identification of SAB peptides from plasma membrane preparations by proteomic approaches⁴³. Further, SAB-3xYpet accumulated in small patches at the nuclear envelope where it co-labelled with microtubules marked by

mCherry-TUA5 during mitotic prophase (Fig. 9i). At the cell cortex, SAB-3xYpet did not precisely co-localize with PPB microtubules but consistently closely associated with them in the majority of prophase cells analysed (91%, 84/92) (Fig. 9i, arrowheads; Supplementary Fig. S5a–f). Strikingly, SAB-3xYpet was also found in patches along mitotic spindle microtubules (Fig. 9j,k), located to cell plate membranes from early to late stages of cell plate formation (Fig. 9l–n), and subsequently remained at domains of apical and basal membranes of dividing cells (Fig. 9e,n). These findings were confirmed in co-labelling studies with rhodamine phalloidin for F-actin staining in aldehyde-fixed cells (Fig. 9o–t) and by co-labelling of the KNOLLE cell plate syntaxin with SAB-3xYpet at the cell plate (Fig. 9u). In elongating epidermal cells, SAB-3xYpet distributed more evenly in endomembrane compartments of unknown identity throughout the cytosol (Fig. 9b). In more differentiated cells, where SAB-3xYpet expression was very low and just detectable above background, SAB-3xYpet compartments were

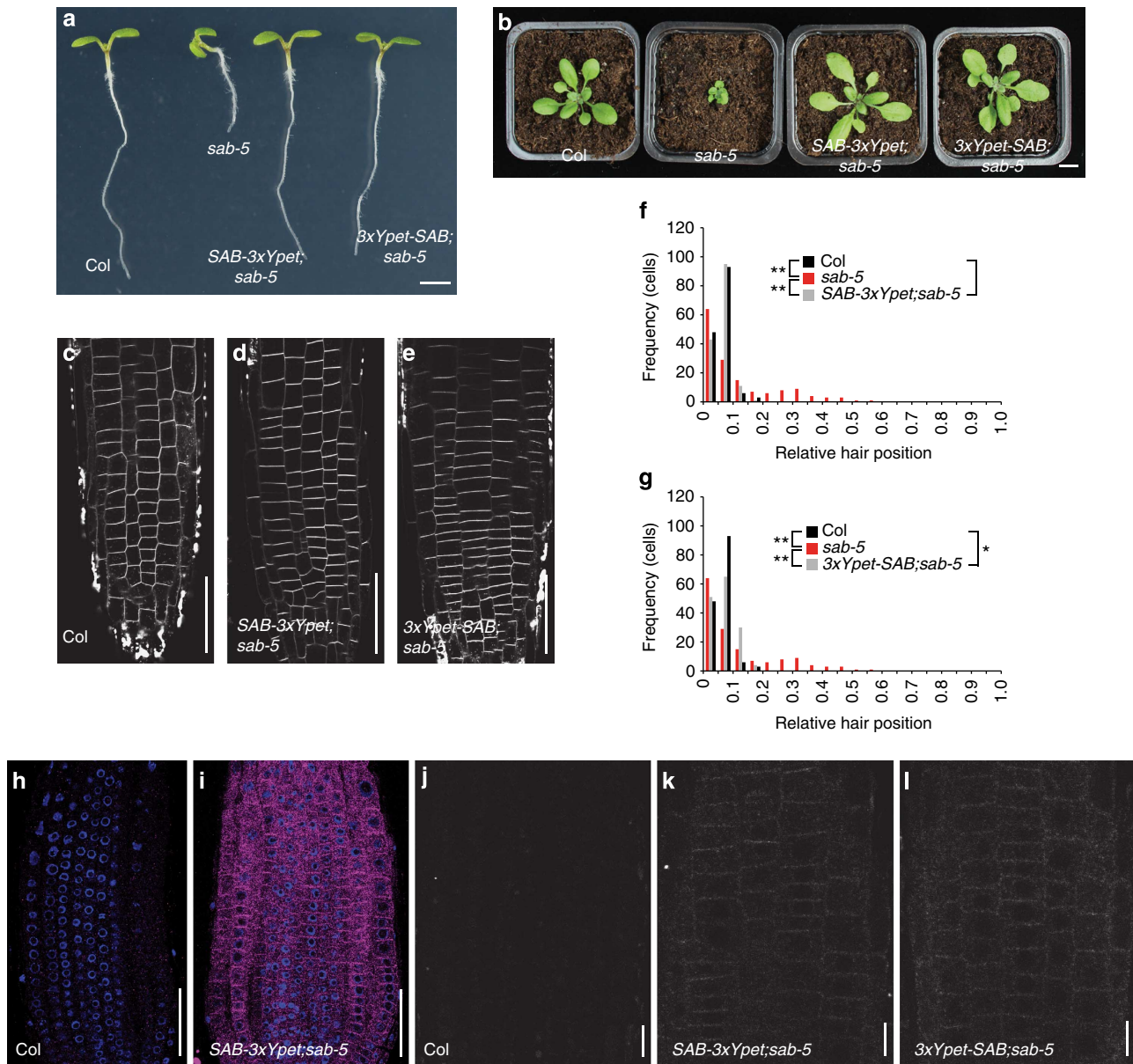


Figure 8 | SAB-3xYpet and 3xYpet-SAB rescue *sab-5* phenotypes and display identical localization. (a) Five-day-old seedlings, (b) 21-day-old plants of Col, *sab-5*, *SAB-3xYpet;sab-5* and *3xYpet-SAB;sab-5*. Note, rescue of *sab-5* growth defects. (c–e) Cell division orientation in root meristem of 5-day-old (c) Col, (d) *SAB-3xYpet;sab-5* and (e) *3xYpet-SAB;sab-5* seedlings. Cells outlined by FM4-64 fluorescence. (f,g) Quantitative analysis of planar polarity in (f) *SAB-3xYpet;sab-5* and (g) *3xYpet-SAB;sab-5* compared with Col and *sab-5* is displayed as relative root hair position similar to Fig. 1c. ** $P=0.000$ Col versus *sab-5*; $P=0.422$ Col versus *SAB-3xYpet;sab-5*; ** $P=0.000$ *sab-5* versus *SAB-3xYpet;sab-5*; * $P=0.019$ Col versus *3xYpet-SAB;sab-5*; ** $P=0.000$ *sab-5* versus *3xYpet-SAB;sab-5* by K-S test, $n=150$ cells from 30 roots per genotype. Note, (f) full rescue of *sab-5* planar polarity defects by *SAB-3xYpet* and (g) partial rescue by *3xYpet-SAB*. (h,i) Expression of *SAB-3xYpet* throughout the root meristem was detected by immunolabelling with anti-GFP antibody (magenta), DAPI (blue), of (h) Col and (i) *SAB-3xYpet;sab-5* seedlings. Images are transversal sections showing *SAB-3xYpet* signal in all cell layers. (j–l) Live imaging of (j) Col, (k) *SAB-3xYpet;sab-5* and (l) *3xYpet-SAB;sab-5* seedlings showing indistinguishable subcellular localization of *SAB-3xYpet* and *3xYpet-SAB* in root meristematic epidermal cells. Scale bars, 2 mm (a), 10 mm (b), 50 μm (c–e,h,i), 10 μm (j–l).

present, although not much enriched, at sites of root hair initiation before morphological outgrowth (Fig. 9v,w). Taken together, we show that SAB localizes to plasma membrane domains, preferentially but not exclusively to apical and basal plasma membranes of meristematic cells, at the nuclear periphery, flanking the PPB at the onset of mitosis, to mitotic spindles, to cell plate membranes as well as to as yet unidentified endomembrane compartments. Thus, SAB is present in most root tip cells including dividing, elongating and differentiating epidermal cells, consistent with its functions in epidermal cells reported here.

Discussion

Our study unravels new roles for the large SAB protein related to uncharacterized proteins found throughout eukaryotes. We report important functions for SAB in PPB, spindle, phragmoplast and cell division plane orientation, cortical microtubule orientation and planar polarity establishment. Moreover, we uncover biological functions of SAB in cell and planar polarity that it shares with CLASP. A role for CLASP function during microtubule-dependent PIN2 polarity establishment in cortical cells and PIN2 abundance modulated by endocytosis has recently attracted attention^{18,19}. Although SAB and CLASP do not

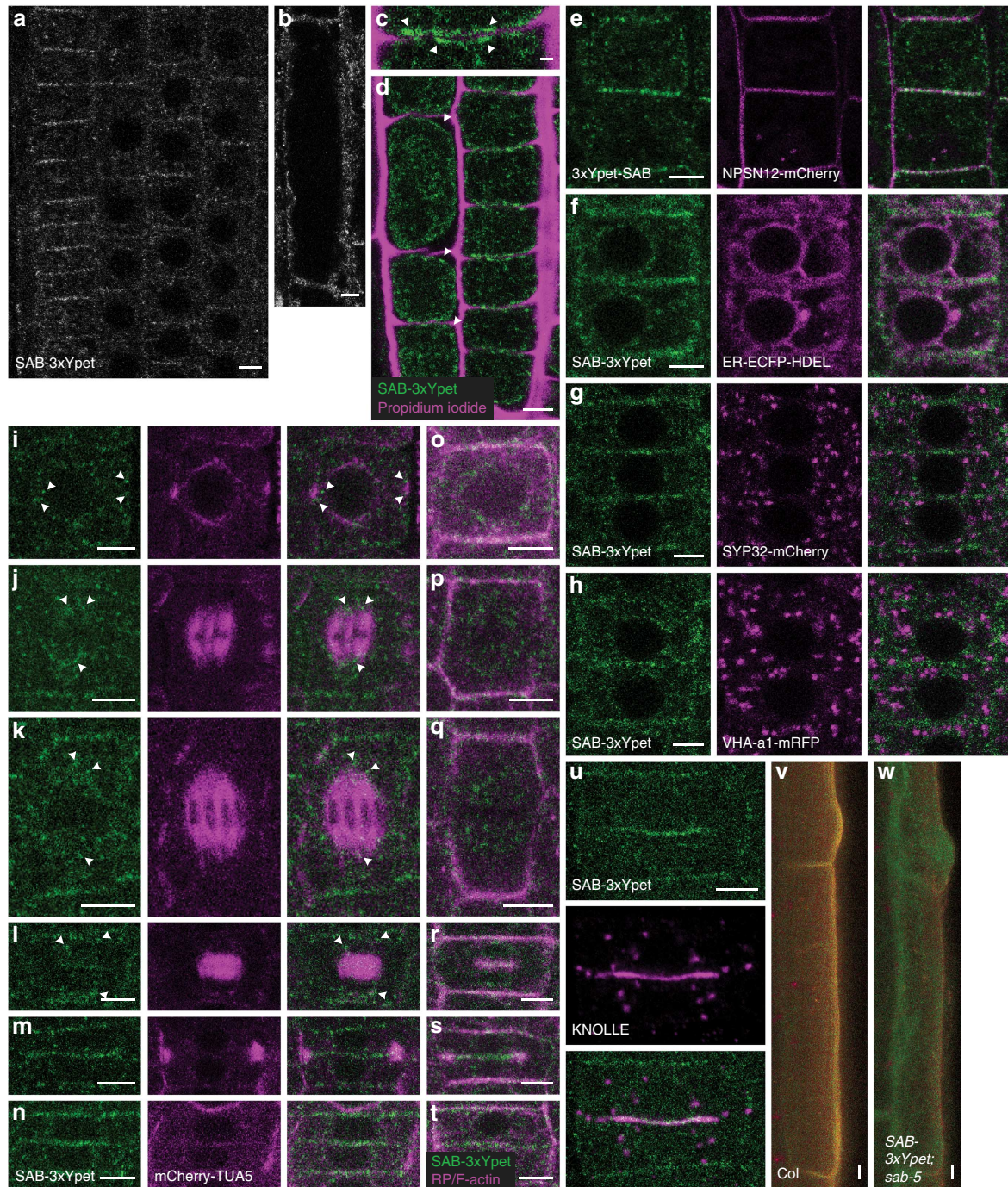


Figure 9 | SAB subcellular localization. (a–h,v,w) Live imaging of functional SAB-3xYpet or 3xYpet-SAB in root epidermal cells of 5-day-old seedlings. (a,b) SAB-3xYpet in *sab-5* background detected in (a) meristematic cells and (b) elongating cells. (c,d) Onset of plasmolysis in 5-day-old, *SAB-3xYpet; sab-5* seedling root co-labelled for SAB-3xYpet (green) and cell wall stain propidium iodide (magenta). Note, (c) apical and basal membrane domain labelling (arrowheads) and (d) separation of SAB-3xYpet from cell wall (arrowheads). (e–h) Meristematic root epidermal cells. (e) 3xYpet-SAB (green) co-localizes with plasma membrane marker NPSN12-mCherry/WAVE131R (magenta). (f–h) SAB-3xYpet (green) co-detected with (f) ER marker ER-ECFP-HDEL (magenta), (g) Golgi marker SYP32-mCherry/WAVE22R (magenta) and (h) TGN marker VHA-a1-mRFP (magenta). Merged channels to the right in e–h. Note, (f) little co-localization and (g,h) no co-localization when compared with e. (i–t) SAB-3xYpet (green) (i–n) co-expressed with mCherry-TUA5 (magenta) and (o–t) co-labelled with rhodamine phalloidin (magenta) for F-actin visualization (RP/F-actin) in paraformaldehyde-fixed roots. (i) Prophase. SAB-3xYpet and mCherry-TUA5 fluorescence around the nuclear envelope. Note, association of SAB-3xYpet (arrowheads) with PPB but no direct co-localization (see also Supplementary Fig. S5). (o) Late prophase. SAB-3xYpet and RP/F-actin. (j,k) SAB-3xYpet localization at mitotic spindles preferentially towards the periphery (arrowheads) in (j,p) metaphase and (k,q) anaphase. (l,r) Late telophase. (l) SAB-3xYpet in centre of phragmoplast at early cell plate and at remaining spindle microtubules (arrowheads). (r) SAB-3xYpet co-labelling with F-actin at early cell plate. (m,s) Late cytokinesis. SAB-3xYpet at cell plate co-labelling with (m) peripheral phragmoplast microtubules and (s) peripheral phragmoplast F-actin. (n,t) End of cytokinesis. SAB-3xYpet at transversal (apical, basal) plasma membranes. (u) anti-KNOLLE cell plate marker immunofluorescence (magenta) and SAB-3xYpet (green) fluorescence. Channel merge (lower panel) indicates co-localization at cell plate. (v,w) Elongated epidermal cells undergoing hair initiation and bulge outgrowth, visualized by colour-coded spectral lambda scan between 416 and 686 nm. Ypet-specific fluorescence, green. (v) Wild type Col. (w) Genomic *SAB-3xYpet; sab-5*. Images in a–w acquired with LSM780 32-channel gallium arsenide phosphide detector array. Scale bars, 5 μ m (a,b,d–x), 1 μ m (c).

appreciably affect apical epidermal PIN2 polarity, we uncover that CLASP mediates establishment of planar polarity of ROP and root hair positioning, and we confirm a previously reported role of CLASP in PPB orientation^{15,16}. Intriguingly, however, our results unravel that *sab* mutations perturb all investigated processes more strongly than *clasp* mutations. *sab* affects PPB, spindle and phragmoplast orientation as well as planar root hair polarity more strongly than *clasp*, and shows an epistatic interaction with *clasp*. Synergistic action of *SAB* and *CLASP* in controlling root length and trichome branching may reflect additional nonlinear interaction, including potential feedback regulation. Alternatively, synergistic action can be interpreted by interaction of *SAB* and *CLASP* with additional partners during these two processes. However, during PPB, spindle and phragmoplast orientation as well as planar polarity in root epidermal cells, *SAB* and *CLASP* act sequentially. Moreover, *SAB* likely acts upstream of *CLASP* considering the misorientation of CLASP-labelled PPBs observed in *sab*, the stronger phenotypes of *sab* mutants and the epistatic relationship of *sab* over *clasp*. Hence, our observations mechanistically link *SAB* function to CLASP-guided cortical microtubule organization during these processes. We further describe a newly observed bipolar arrangement of longitudinally growing microtubules at later stages of root hair cell elongation. Although striking and similar to the bipolar arrangement recently observed in hypocotyl cells³⁶, the functional importance of this dynamic bipolar reorganization, and how it may affect polar site selection during root hair initiation, remains to be determined. Further, we find that *sab* is epistatic to *clasp* during polar placement of ROP protein patches at sites of hair initiation where we observe cortical microtubule reorganization before morphological onset of hair outgrowth. Earlier observations have implicated microtubules in tip growth of different cell types in various organisms^{14,44–46}, and radial microtubule alignment has been observed, for example, in tips of moss protonemata⁴⁴ as well as in conifer pollen tubes⁴⁵. In addition, microtubule dynamics are known to have a function in directing the growth of and limiting the number of growth sites in root hairs^{46,47}. Our work also points out a role for microtubule reorganization in polarity of root hair cells. However, we report that microtubules are involved earlier than previously described, namely, during selection of the site of root hair initiation. This suggests that the microtubule cytoskeleton acts both in determining planar polarity of hair cell differentiation and in maintaining polar tip growth of root hairs. It remains to be determined how *SAB* affects microtubule reorganization at the molecular level because the genetic interactions observed between *SAB* and *CLASP* may not necessarily reflect direct interaction at the protein level. Yet, *SAB*-3xYpet localized to the perinuclear region from where microtubules radiate towards the PPB as well as adjacent to the PPB, suggesting that *SAB* may be, directly or indirectly, involved in nucleation or guidance of PPB microtubules. This localization does, however, not match exactly the distribution of *CLASP*, which directly co-localizes with PPB microtubules at cell edges and binds to microtubule plus ends^{20,21}. This suggests that the observed genetic interactions may reflect an indirect or transient interaction within the same pathway. The *SAB* protein localizes to spindle microtubules from early prophase, and later on is observed close to the spindle periphery consistent with our findings that *SAB* is required for spindle and phragmoplast orientation. Further, the accumulation of *SAB* at cell plate membranes in the centre of the phragmoplast and on apical and basal plasma membranes opens the door for future studies on the role of *SAB* at these sites. Hence, our work paves the way to elucidating the molecular function of *SAB* in microtubule reorganization during cell division plane orientation, cell and planar polarity formation in plants. It also encourages

further studies on the connection between *SAB*-related proteins and the microtubule cytoskeleton. Future studies may now address what proteins the large membrane protein *SAB* interacts with at the molecular level and which of the homology regions observed in *SAB*-like proteins throughout eukaryotes may be required for such interactions. Interestingly, the human genome encodes a single *SAB*-related predicted 2,235 amino-acid-long protein of unknown function named KIAA0100, which is overexpressed in human cancers and also known as, for example, *breast cancer overexpressed1* or *monocytic leukaemia-associated antigen22* (refs 48–51). Hence, our findings linking *SAB* to *CLASP*-mediated microtubule organization may provide a stepping stone for functional analysis of *SAB*-related proteins during eukaryotic development and for dissecting their potential role in human cancer.

Methods

Plant growth conditions. Medium and growth conditions were as described⁴. In brief, seeds were surface sterilized and stratified at 4 °C for 3 days before plating on MS plates (1 × MS medium, 1% sucrose, 0.8% plant agar, 1 M morpholinoethanesulphonic acid, pH 5.7). Seedlings were grown vertically at 23 °C day and 18 °C night under 16 h light/8 h dark photoperiod and subjected to analysis after 5 days.

Plant material and genotyping. *Arabidopsis thaliana* ecotype Columbia (Col-0) was employed as a wild type and as background for the *kuq* mutant; the following T-DNA insertion lines from the SALK collection⁵² were obtained from the Nottingham *Arabidopsis* Stock Centre: *sab-5* (stock number N608709), *sab-6* (N552995), *sab-7* (N623771) and *sab-8* (N512897). All above *sab* alleles, with the exception of *sab-7*, were unable to self-fertilize and produced 5–10 seeds per silique on pollination with wild-type pollen. Lines were maintained as heterozygotes and molecular genotyping was used to identify plants carrying mutant alleles. Other previously described mutants and transgenic lines were provided by the Nottingham *Arabidopsis* Stock Centre or corresponding authors of the cited publications: *pPEN3:PEN3-GFP*⁵³, *p35S:GFP-BASL*²⁴, *clasp-1* (refs 15,16) (N620061), *clasp-2* (refs 15,16) (N583034), *p35S:mCherry-TUA5* (refs 32,33), *p35S:H2B-YFP*⁵⁴, *pCLASP:GFP-CLASP*²¹, *p35S:EB1a-GFP*⁵⁵, *pGL2:NTF*⁵⁴, *pPIP5K3:PIP5K3-YFP*³⁷, *pUBQ10:NSP12-mCherry/WAVE131R*⁴¹, *pUBQ10:SY32-mCherry/WAVE22R*⁴¹ and *VHA-a1-mRFP*⁴². Other mutant and transgene combinations were generated in this study. Primers for PCR genotyping of mutants are listed in Supplementary Table S3.

Immunofluorescence and CLSM. Whole-mount immunolabelling of roots was performed as described⁴. Antibody dilutions were the following: rabbit anti-ROP 1:25 (ref. 8); rabbit anti-PIN2 1:400 (ref. 55); mouse anti- α -tubulin DM1A 1:200 (Santa Cruz, Sc-32293); rabbit anti-GFP 1:1,000 (Torrey Pines, TP-401); rabbit anti-KNOLLE 1:4,000 (ref. 56); DY649 donkey anti-rabbit 1:800 (Jackson ImmunoResearch) for anti-ROP, anti-PIN2, anti-GFP; DyLight633 donkey anti-rabbit 1:100 (Agrisera, AS122034) for anti-KNOLLE; TRITC donkey anti-mouse 1:150 (Jackson ImmunoResearch). Donkey secondary antibodies for multilabelling pre-absorbed to crossreacting species were employed. DNA was stained with 4',6-diamidino-2-phenylindole (DAPI) (1 μ g ml⁻¹, Sigma). Imaging of immunolabelled or live roots was carried out using either a Leica TCS SP2 AOBs (Leica) spectral confocal laser scanning microscopy (CLSM) system mounted on an Leica DM IRE2 inverted microscope or a Zeiss LSM780 spectral CLSM system equipped with a 32-channel gallium arsenide phosphide detector array and mounted on a Zeiss Axio observer Z1 inverted microscope. Laser excitation lines, emission filters and acquisition modes for all fluorophore combinations are listed in Supplementary Table S4. Oil-corrected Plan-Apochromat \times objectives, numerical aperture 1.4 (HCX PL APO 63.0 \times 1.40 OI BD UV, Leica; or DIC M27, Zeiss) were used for immunolabelling studies. For live imaging, a water-corrected C-Apochromat 40 \times objective, numerical aperture 1.2 (M27, Zeiss) was used. It was not possible to detect 3xYpet-SAB and SAB-3xYpet fluorescent fusions with a Leica SP2 confocal microscope in live imaging studies because of extremely low intensity of the signal. Hence, all imaging of these lines was carried out with a Zeiss LSM780 microscope. It was however possible to detect SAB-3xYpet and 3xYpet-SAB with a Leica SP2 microscope after immunolabelling with anti-GFP antibody (Torrey Pines). Images were processed and analysed using ZEN2010 (Zeiss), ImageJ (<http://www.imagej.nih.gov/ij/>) or Adobe Photoshop CS4 (Adobe Systems), and assembled in Adobe Illustrator CS3 (Adobe Systems).

Analysis of root hair position and trichoblast length. Quantitative microscopic analysis of root hair position and cell length was performed in three independent experiments as described⁴. Statistical analysis employed non-parametric Kolmogorov–Smirnov (K–S) test and two-tailed *t*-test.

Quantitative analysis of ROP positioning. Relative ROP position in trichoblasts before hair initiation was determined by immunolocalization as described⁴. Measurements were performed on $n = 50$ cells per genotype, from 8 to 22 roots. Images were analysed using Leica Application Suite Advanced Fluorescence software (Leica).

Scanning electron microscopy of leaf trichome orientation. Growth of *sab* mutants was significantly slower compared with wild-type plants. To analyse leaves at a similar developmental stage, the third true leaf from 21-day-old *sab* plants was compared with the third true leaf from 14-day-old wild-type plants that did not obviously differ in trichome orientation from 21-day-old wild-type plants. Leaves were fixed in 2.5% glutaraldehyde in sodium cacodylate buffer overnight at room temperature. To keep the leaves submerged in the solution, the fixation was carried out in a desiccator with a low under-pressure to take away trapped air. Fixed material was dehydrated in increasing ethanol concentrations, up to pure ethanol, and was thereafter dried from liquid CO₂ using standard critical point drying technique (Polaron E3000 CPD apparatus, Quorum Technologies Ltd, Ashford, UK). Dried specimens were attached to specimen holders using adhesive carbon tape and thereafter coated with ~15 nm gold in an evaporation system. Microscopy was performed in a scanning electron microscope running at standard conditions (Carl Zeiss SMT/Cambridge Instruments 360iXP, Cambridge, UK) and micrographs were recorded at standardized magnifications and locations on the leaves. Trichome orientation was investigated in a rectangle of 2 mm × 1.5 mm in the centre of the leaf adaxial surface. Angles between the proximal-distal leaf axis and the trichome's first branch were measured on scanning electron microscope images using ImageJ.

Isolation and positional cloning of *kuq*. The *kuq* mutant was isolated in a genetic screen of 5-day-old seedlings for aberrant planar polarity of root hair positioning. A population of ~20,000 M₂ seedlings obtained from ~2,500 fast-neutron-mutagenized M₁ plants (Col-0 ecotype, Lehle Seeds) were grown vertically and screened by stereomicroscopy. *kuq* was characterized by a more random root hair position along epidermal cells, shorter and radially swollen roots and bent cotyledons. The semi-sterile *kuq* mutant was fertilized with Col-0 pollen and produced five to eight seeds, which were subjected to further analyses. The *kuq* phenotype segregated at 27% ($n = 496$) after backcrossing, indicating that it was caused by a single, recessive mutation. *kuq* was crossed to Landsberg *erecta* (*Ler*) to generate a mapping population, and genomic DNA (gDNA) was extracted from 1,298 F₂ seedlings displaying the *kuq* phenotype and used for mapping by positional cloning⁵⁷. SSLP and CAPS molecular markers were generated as described⁵⁷ and by using the Monsanto *Arabidopsis* Polymorphism Collection (<http://www.arabidopsis.org/browse/Cereon/index.jsp>), and the mutation was mapped to a 480-kb interval on chromosome 1 (Fig. 2). Analysis of T-DNA insertion lines in genes within this interval suggested the *SABRE* (*SAB*) gene as the strongest candidate, with 9 T-DNA lines whose homozygous seedlings looked indistinguishable from *kuq* mutants. The entire ~14.5 kb *SAB* genomic region was PCR amplified from *kuq* mutants and sequenced with three times coverage. This revealed a single cytosine deletion in the 17th exon of the *SAB* gene, at position 6,592 (of 7,824) of the coding sequence. The mutation caused a frame shift that was calculated to introduce a stop codon at position 6,617–6,619, truncating the predicted *SAB* protein after amino acid 2,205 (of 2,607). A CAPS marker designed over the mutated site physically confirmed the nucleotide deletion and allowed molecular genotyping of *kuq* mutants (see Supplementary Table S3).

RT-PCR analysis. Total RNA was extracted from roots of 5-day-old seedlings employing the RNeasy Plant Mini Kit (Qiagen) according to manufacturer's instructions. Two biological replicates were analysed for each mutant and the respective wild-type control. RNA was purified with the Ambion DNA-free Kit (Ambion), precipitated with LiCl and resuspended in diethyl pyrocarbonate-treated H₂O. cDNA was synthesized using iScript cDNA Synthesis Kit (Bio-Rad) and used for semiquantitative RT-PCR analysis with primer pairs spanning the T-DNA insertion (or single-nucleotide deletion), and primer pairs located respectively at the 5'- and 3'-end of the *SAB* gene (Supplementary Table S3 for primer sequences). Primer pairs were designed to span introns to identify potential gDNA contaminations. Primers amplifying the *ELONGATION FACTOR 1- α* (*EF1- α*) or *ADENINE PHOSPHORIBOSYL TRANSFERASE 1* (*APT1*) genes were used as controls. Reactions were carried out with 34 cycles for T-DNA insertion spanning primers (22 cycles for *EF1- α* primers) and 35 cycles for primers located close to the 5'- or 3'- end of the *SAB* gene (35 and 40 cycles for *APT1* primers, respectively).

Analysis of *SAB* evolutionary conservation. Searches for proteins with similarity to *SAB* were performed with Blastp version 2.2.28+ (<http://www.blast.ncbi.nlm.nih.gov/blast/Blast.cgi>) with default parameters using full *SAB* sequence (At1g58250.1) against non-redundant protein sequences database. Alignment of *Saccharomyces cerevisiae* and *Schizosaccharomyces pombe* proteins was achieved after second PSI-BLAST iteration. Full sequences of *SAB*-related proteins from selected species were aligned with MUSCLE version 3.8.31 (<http://www.ebi.ac.uk/Tools/services/web/toolform.ebi?tool=muscle>). Output phenogramme generated

from second iteration was visualized with PhyloDendron Phylogenetic tree printer (<http://www.iubio.bio.indiana.edu/treeapp/treeprint-form.html>).

Trichome branching analysis. Measurements of trichome branching were performed as described¹⁵. Third true leaf of 21-day-old plants was observed with a Leica MZ 9.5 stereomicroscope (Leica), and number of branches was counted for all trichomes on adaxial leaf surface. Number of leaves (plants) analysed are as follows: 10 for Col-0, 12 for *clasp-1*, 16 for *sab^{kuq}*, 16 for *sab-5* and 16 for *sab-5;clasp-1*.

FM4-64 staining. Seedlings were incubated in 1 × MS medium with 25 μ M FM4-64 (Molecular Probes) for 5 min on ice. After two washes with 1 × MS medium on ice, seedlings were mounted on cover slips in 1 × MS medium.

Live imaging of microtubules and nuclei during cell division. Wild-type looking and *sab-5* seedlings expressing mCherry-TUA5 (ref. 32) and H2B-YFP⁵⁴ were imaged live. A region of 53.14 μ m × 53.14 μ m centred on a meristematic cell in prophase (displaying clear PPB) was visualized at intervals of 1 min throughout cell division. For each time point, Z stacks of six optical sections at 0.46 μ m distance were acquired, and the image closest to the centre of the cell was selected. Imaging windows and planes were constantly adjusted to account for movement of roots in X-, Y- and Z-direction. Images of each time point were aligned using ImageJ Stackreg plugin (<http://www.bigwww.epfl.ch/thevenaz/stackreg/>) before movie assembly.

Analysis of mitotic figure orientation. Seedlings were labelled with mouse anti- α -tubulin antibody (Santa Cruz). Z stacks were acquired from meristematic cells in prophase, metaphase and late cytokinesis, and images closest to the centre of the cell were selected. For each cell, length of the longitudinal cell edges and distances between the transversal cell edges and the points where the PPB ring or phragmoplast touched the longitudinal edges were measured. Deviation of PPB, mitotic spindle and phragmoplast orientation from the transversal central axis (midplane) of the cell was indicated by the absolute value derived by the following formula: $100 - (\text{distance between transversal edge and mitotic structure} / \text{total length of longitudinal edge} \times 200)$. A mean of 0% between the two values calculated for a cell (one corresponding to each side) indicated a structure passing through the midplane, whereas 100% was one tracing a diagonal of the cell. Higher deviations occurred rarely (2.5% of 720 cells in total) and were considered as 100% for further analysis. Box-and-whisker plots were used to visualize deviation from the midplane in the 60 cells examined for each genotype and mitotic stage: for each data set they display median, upper quartile (blue box), lower quartile (red box), maximum (upper whisker) and minimum (lower whisker) of the population.

Live imaging of cortical microtubules. Cortical microtubules were analysed in epidermal cells of seedlings expressing mCherry-TUA5 (ref. 32) and AtEB1a-GFP³⁵ or PIP5K3-YFP³⁷. For movies of microtubule growth, Z stacks of planes intersecting the periclinal face of the cell 1 μ m apart (0.51 μ m in elongating wild-type cells) were imaged every 5 s for 2.5 min. Maximum intensity projections of each time point were used to assemble movies. For images of cortical microtubules in cells about to initiate outgrowth of a root hair, Z stacks of planes at 0.46 μ m distance intersecting the periclinal face of the cell were acquired and employed to generate maximum intensity projections. Relative PIP5K3-YFP position was determined measuring the distance between basal trichoblast membrane and basal end of PIP5K3-YFP patch on the upper cell face and dividing it by total cell length. Measurements were performed on $n = 50$ cells per genotype from 39 to 41 roots.

Microtubule orientation measurements. Seedlings with wild-type or *sab-5* phenotype expressing the atrichoblast marker pGL2:NTF⁵⁴ and mCherry-TUA5 (ref. 32) were imaged live. Trichoblasts were identified by absence of pGL2:NTF. Z stacks of planes at 0.45 μ m distance were acquired on the periclinal face from either meristematic cells of 13–18 μ m or elongated cells of 26–36 μ m cell length. Maximum intensity projections were used to measure the angle of microtubules with respect to the root growth axis.

Generation of *SAB-3xYpet* and *3xYpet-SAB* lines. A 3xYpet tag was fused to *SAB* at either the C- or the N-terminus by recombining⁵⁸. The JAtY clone 63C14, purchased from the John Innes Centre (Norwich, UK), was selected based on bacterial artificial chromosome end sequence information from the *Arabidopsis thaliana* Integrated Database, <http://www.atidb.org/cgi-perl/gbrowse/atibrowse/>. In this clone, the *SAB*-coding region is preceded and followed by 36 and 4.5 kb of gDNA, respectively. The JAtY transformation-competent bacterial artificial chromosome was transferred to *Escherichia coli* strain SW105, kindly provided by Dr N. Copeland (Mouse Cancer Genetics Program, National Cancer Institute Frederick, Frederick, MD, USA)⁵⁸. A recombining cassette was generated by inserting the ampicillin resistance gene flanked by flippase recognition sites at the 3'-end of the codon-optimized 3xYpet tag³⁸ (cassette available from the

Arabidopsis Biological Resource Center, stock number CD3-1727). The cassette was amplified by PCR using two long recombining primers (Supplementary Table S3): the forward primer included 50 nucleotides homologous to the region upstream of the 3xYpet insertion point (until right after the first codon of the *SAB* gene for the N-terminal fusion and before the STOP codon for the C-terminal fusion); the reverse primer included 50 nucleotides homologous to the region downstream of the insertion point (ending just after the first codon or before the STOP codon of *SAB*, respectively). Cassette recombination into the JATY clone was performed as described³⁸, and the *Amp^R* marker was removed on induction of the *Flippase* gene expression by arabinose. Constructs were sequenced and respective transformation-competent bacterial artificial chromosome clones transformed into *Agrobacterium tumefaciens* GV3101, which was used to transform *sab-5* heterozygous *Arabidopsis* plants by floral dipping^{38,59}. Transformants were selected by Basta and further screened by PCR, ensuring presence of the *sab-5*-mutant allele, of the tagged *SAB* gene, and of the *SacB* gene (for primer sequences Supplementary Table S3). *SacB* lies close to the T-DNA left border and its presence confirmed transfer of at least one full copy of the T-DNA to the plant genome³⁸. T₂ seedlings were analysed for fluorescence using a Zeiss LSM780 confocal microscope. Out of 12 *SAB-3xYpet* lines analysed, 7 displayed a very weak but identical fluorescent signal. Out of 10 3xYpet-*SAB* lines, 9 showed the same pattern of fluorescence, indistinguishable from *SAB-3xYpet* lines. One line was selected for each construct and T₂ plants homozygous for the *sab-5* allele and the *SAB* transgene were identified. Offspring of these plants was used for all further analyses and genetic crosses.

Plasmolysis. Plasmolysis was performed as described⁶⁰. Seedlings were incubated in 1 ml of 0.8 M mannitol for 2 h under gentle agitation, stained for 30 s in 10 µg ml⁻¹ propidium iodide in 0.8 M mannitol, mounted on cover slips in the same medium and immediately imaged.

Generation of ER-ECFP-HDEL marker. The binary vector pGreenII0229 (ref. 61; obtained from the John Innes Centre, Norwich) was modified by adding a *Cauliflower mosaic virus* 35S promoter (derived from the pSK36 vector⁶²) and a *Nopaline synthase* terminator between the *Bam*HI and *Spe*I, and at the *Not*I site of the multiple cloning site, respectively. The resulting vector was named p235S. ER signal peptide of *Arabidopsis Basic chitinase* (At3g12500) was amplified from gDNA using primers CHTTTPFAscl and CHTTTPRSpeI. PCR product was digested with *As*cl and *Spe*I and cloned into the corresponding sites of the p235S vector, generating the p235S-TP construct. Enhanced cyan fluorescent protein (ECFP) coding sequence was amplified from the pECFP-C1 vector (Clontech) using primers CFPFSpeI and CFPERNotI, which introduced the coding sequence for the ER-retention signal peptide HDEL before the stop codon. PCR product was digested with *Spe*I and *Not*I and subcloned into the corresponding sites of the p235S-TP vector. After sequencing with 35SF and tNOSR primers, the resulting construct was transferred to *A. tumefaciens* strain C58C1 and used to transform *Arabidopsis Col-0* plants by floral dipping⁵⁹. T₁ transgenic plants were selected by Basta. Primer sequences are listed in Supplementary Table S3.

Visualization of SAB together with microtubules or F-actin. Seedlings expressing *SAB-3xYpet* or *SAB-3xYpet* and mCherry-TUA5 were fixed for 40 min in PME buffer (50 mM piperazine-1,4-bis(2-ethanesulfonic acid), 2 mM MgSO₄, 5 mM ethylene glycol-bis(β-aminoethylether)-N,N,N',N'-tetraacetic acid, pH 6.9) supplemented with 0.1% Triton X-100 and 2% paraformaldehyde as described⁶³. After three washes with PME buffer, seedlings were either mounted on cover slips in PME buffer and immediately imaged (for seedlings expressing *SAB-3xYpet* and mCherry-TUA5) or, for visualization of F-actin, mounted in 2% rhodamine phalloidin (Molecular Probes) in PME buffer and incubated 50 min in dark before imaging. To assess *SAB-3xYpet* localization relative to PPB, two sections (one through the middle of the cell and one 4–5 µm apart) were evaluated.

Lambda scan of root hair initiation sites. Lambda scans of trichoblasts undergoing hair initiation were captured from live *Col-0* seedlings and seedlings expressing *SAB-3xYpet*, using a Zeiss LSM780 confocal microscope. On excitation at 514 nm, 32 images were acquired with narrow detection windows covering the spectral region between 416 nm and 686 nm, in Z stacks of planes at a distance of 2 µm. Maximum intensity Z projections were generated and lambda stacks were visualized in wavelength-coded colour view employing ZEN2010 (Zeiss) software.

Statistical analysis. Positioning of root hairs, ROP or PIP5K3-YFP patches along trichoblasts, and cell division and microtubule orientation angles did not follow a normal distribution. Thus, significance of differences between distributions was tested with non-parametric, two-sample Kolmogorov–Smirnov test (http://www.physics.csbsju.edu/stats/KS-test.n.plot_form.html), which considers both distributions' location and shape. Distributions of $n = 150$ or 50 trichoblasts from root hair and ROP or PIP5K3-YFP position measurements, respectively, of $n = 60$ cells per mitotic stage, and of $n = 673$ –802 or 578–520 cortical microtubules were analysed with significance level $P < 0.05$. Differences in trichome orientation were

analysed by F-test (Microsoft Excel), with $n = 174$. Measurements of GFP-BASL polar localization and trichome branching were analysed by Fisher's exact test (<http://www.quantitativeskills.com/sisa/statistics/fiveby2.htm>), with populations of $n > 187$ and $n > 400$, respectively, with significance level $P < 0.05$. Analysis of trichoblast length was performed by two-tailed, unpaired *t*-test with equal variance (computed with Microsoft Excel), with $n = 3$ average values of independent experiments and significance level $P < 0.05$.

References

- Goodrich, L. V. & Strutt, D. Principles of planar polarity in animal development. *Development* **138**, 1877–1892 (2011).
- Bertet, C. & Lecuit, T. Planar polarity and short-range polarization in *Drosophila* embryos. *Semin. Cell Dev. Biol.* **20**, 1006–1013 (2009).
- Masucci, J. D. & Schiefelbein, J. W. The *rhod6* mutation of *Arabidopsis thaliana* alters root-hair initiation through an auxin- and ethylene-associated process. *Plant Physiol.* **106**, 1335–1346 (1994).
- Fischer, U. *et al.* Vectorial information for *Arabidopsis* planar polarity is mediated by combined *AUX1*, *EIN2*, and *GNOM* activity. *Curr. Biol.* **16**, 2143–2149 (2006).
- Hülkamp, M., Misra, S. & Jürgens, G. Genetic dissection of trichome cell development in *Arabidopsis*. *Cell* **76**, 555–566 (1994).
- Wu, J., Roman, A. C., Carvajal-Gonzalez, J. M. & Mlodzik, M. Wg and Wnt4 provide long-range directional input to planar cell polarity orientation in *Drosophila*. *Nat. Cell Biol.* **15**, 1045–1055 (2013).
- Ikeda, Y. *et al.* Local auxin biosynthesis modulates gradient-directed planar polarity in *Arabidopsis*. *Nat. Cell Biol.* **11**, 731–738 (2009).
- Molendijk, A. J. *et al.* *Arabidopsis thaliana* Rop GTPases are localized to tips of root hairs and control polar growth. *EMBO J.* **20**, 2779–2788 (2001).
- Jones, M. A. *et al.* The *Arabidopsis* Rop2 GTPase is a positive regulator of both root hair initiation and tip growth. *Plant Cell* **14**, 763–776 (2002).
- Carol, R. J. *et al.* A RhoGDP dissociation inhibitor spatially regulates growth in root hair cells. *Nature* **438**, 1013–1016 (2005).
- Fu, Y., Xu, T., Zhu, L., Wen, M. & Yang, Z. A ROP GTPase signaling pathway controls cortical microtubule ordering and cell expansion in *Arabidopsis*. *Curr. Biol.* **19**, 1827–1832 (2009).
- Xu, T. *et al.* Cell surface- and Rho GTPase-based auxin signaling controls cellular interdigitation in *Arabidopsis*. *Cell* **143**, 99–110 (2010).
- Ringli, C., Baumberger, N., Diet, A., Frey, B. & Keller, B. ACTIN2 is essential for bulge site selection and tip growth during root hair development of *Arabidopsis*. *Plant Physiol.* **129**, 1464–1472 (2002).
- Bao, Y., Kost, B. & Chua, N. H. Reduced expression of alpha-tubulin genes in *Arabidopsis thaliana* specifically affects root growth and morphology, root hair development and root gravitropism. *Plant J.* **28**, 145–157 (2001).
- Kirik, V. *et al.* CLASP localizes in two discrete patterns on cortical microtubules and is required for cell morphogenesis and cell division in *Arabidopsis*. *J. Cell Sci.* **120**, 4416–4425 (2007).
- Ambrose, J. C., Shoji, T., Kotzer, A. M., Pighin, J. A. & Wasteneys, G. O. The *Arabidopsis* CLASP gene encodes a microtubule-associated protein involved in cell expansion and division. *Plant Cell* **19**, 2763–2775 (2007).
- Dhonukshe, P. *et al.* A PLETHORA-auxin transcription module controls cell division plane rotation through MAP65 and CLASP. *Cell* **149**, 383–396 (2012).
- Ambrose, C. *et al.* CLASP interacts with Sorting Nexin 1 to link microtubules and auxin transport via PIN2 recycling in *Arabidopsis thaliana*. *Dev. Cell* **24**, 649–659 (2013).
- Kakar, K., Zhang, H., Scheres, B. & Dhonukshe, P. CLASP-mediated cortical microtubule organization guides PIN polarization axis. *Nature* **495**, 529–533 (2013).
- Galjart, N. CLIPs and CLASPs and cellular dynamics. *Nat. Rev. Mol. Cell Biol.* **6**, 487–498 (2005).
- Ambrose, C., Allard, J. F., Cytrynbaum, E. N. & Wasteneys, G. O. A CLASP-modulated cell edge barrier mechanism drives cell-wide cortical microtubule organization in *Arabidopsis*. *Nat. Commun.* **2**, 430 (2011).
- Strader, L. C. & Bartel, B. The *Arabidopsis* PLEIOTROPIC DRUG RESISTANCE8/ABCG36 ATP binding cassette transporter modulates sensitivity to the auxin precursor indole-3-butyric acid. *Plant Cell* **21**, 1992–2007 (2009).
- Langowski, L., Ruzicka, K., Naramoto, S., Kleine-Vehn, J. & Friml, J. Trafficking to the outer polar domain defines the root-soil interface. *Curr. Biol.* **20**, 904–908 (2010).
- Dong, J., MacAlister, C. A. & Bergmann, D. C. BASL controls asymmetric cell division in *Arabidopsis*. *Cell* **137**, 1320–1330 (2009).
- Buschmann, H. & Lloyd, C. W. *Arabidopsis* mutants and the network of microtubule-associated functions. *Mol. Plant* **1**, 888–898 (2008).
- Benfey, P. N. *et al.* Root development in *Arabidopsis*: four mutants with dramatically altered root morphogenesis. *Development* **119**, 57–70 (1993).

27. Aeschbacher, R. A., Hauser, M. T., Feldmann, K. A. & Benfey, P. N. The *SABRE* gene is required for normal cell expansion in *Arabidopsis*. *Genes Dev.* **9**, 330–340 (1995).
28. Procissi, A. *et al.* *KINKY POLLEN* encodes a SABRE-like protein required for tip growth in *Arabidopsis* and conserved among eukaryotes. *Plant J.* **36**, 894–904 (2003).
29. Yu, H., Luo, N., Sun, L. & Liu, D. HPS4/SABRE regulates plant responses to phosphate starvation through antagonistic interaction with ethylene signalling. *J. Exp. Bot.* **63**, 4527–4538 (2012).
30. Xu, Z. & Dooner, H. K. The Maize *aberrant pollen transmission 1* gene is a *SABRE/KIP* homolog required for pollen tube growth. *Genetics* **172**, 1251–1261 (2006).
31. Marchler-Bauer, A. *et al.* CDD: conserved domains and protein three-dimensional structure. *Nucleic Acids Res.* **41**, D348–D352 (2013).
32. Gutierrez, R., Lindeboom, J. J., Paredes, A. R., Emons, A. M. & Ehrhardt, D. W. *Arabidopsis* cortical microtubules position cellulose synthase delivery to the plasma membrane and interact with cellulose synthase trafficking compartments. *Nat. Cell Biol.* **11**, 797–806 (2009).
33. Sampathkumar, A. *et al.* Live cell imaging reveals structural associations between the actin and microtubule cytoskeleton in *Arabidopsis*. *Plant Cell* **23**, 2302–2313 (2011).
34. Boissnard-Lorig, C. *et al.* Dynamic analyses of the expression of the HISTONE::YFP fusion protein in *Arabidopsis* show that syncytial endosperm is divided in mitotic domains. *Plant Cell* **13**, 495–509 (2001).
35. Chan, J., Calder, G. M., Doonan, J. H. & Lloyd, C. W. EB1 reveals mobile microtubule nucleation sites in *Arabidopsis*. *Nat. Cell Biol.* **5**, 967–971 (2003).
36. Sambade, A., Pratap, A., Buschmann, H., Morris, R. J. & Lloyd, C. The influence of light on microtubule dynamics and alignment in the *Arabidopsis* hypocotyl. *Plant Cell* **24**, 192–201 (2012).
37. Kusano, H. *et al.* The *Arabidopsis* phosphatidylinositol phosphate 5-kinase PIP5K3 is a key regulator of root hair tip growth. *Plant Cell* **20**, 367–380 (2008).
38. Zhou, R., Benavente, L. M., Stepanova, A. N. & Alonso, J. M. A recombineering-based gene tagging system for *Arabidopsis*. *Plant J.* **66**, 712–723 (2011).
39. Zheng, H., Kunst, L., Hawes, C. & Moore, I. A GFP-based assay reveals a role for RHD3 in transport between the endoplasmic reticulum and Golgi apparatus. *Plant J.* **37**, 398–414 (2004).
40. Swarup, R. *et al.* Structure-function analysis of the presumptive *Arabidopsis* auxin permease AUX1. *Plant Cell* **16**, 3069–3083 (2004).
41. Geldner, N. *et al.* Rapid, combinatorial analysis of membrane compartments in intact plants with a multicolor marker set. *Plant J.* **59**, 169–178 (2009).
42. von der Fecht-Bartenbach, J. *et al.* Function of the anion transporter AtCLC-d in the *trans*-Golgi network. *Plant J.* **50**, 466–474 (2007).
43. Benschop, J. J. *et al.* Quantitative phosphoproteomics of early elicitor signaling in *Arabidopsis*. *Mol. Cell Proteomics* **6**, 1198–1214 (2007).
44. Doonan, J. H., Cove, D. J. & Lloyd, C. W. Immunofluorescence microscopy of microtubules in intact cell lineages of the moss, *Physcomitrella patens*. I. Normal and CIPC-treated tip cells. *J. Cell Sci.* **75**, 131–147 (1985).
45. Anderhag, P., Hepler, P. K. & Lazzaro, M. D. Microtubules and microfilaments are both responsible for pollen tube elongation in the conifer *Picea abies* (Norway spruce). *Protoplasma* **214**, 141–157 (2000).
46. Rounds, C. M. & Bezanilla, M. Growth mechanisms in tip-growing plant cells. *Annu. Rev. Plant Biol.* **64**, 243–265 (2013).
47. Bibikova, T. N., Blancaflor, E. B. & Gilroy, S. Microtubules regulate tip growth and orientation in root hairs of *Arabidopsis thaliana*. *Plant J.* **17**, 657–665 (1999).
48. Song, J., Yang, W., Shih, I. M., Zhang, Z. & Bai, J. Identification of BCOX1, a novel gene overexpressed in breast cancer. *Biochim. Biophys. Acta* **1760**, 62–69 (2006).
49. Zhou, F. L., Zhang, W. G., Meng, X., Chen, G. & Wang, J. L. Bioinformatic analysis and identification for a novel antigen MLLAA-22 in acute monocytic leukemia. *Zhongguo. Shi Yan Xue Ye Xue Za Zhi* **16**, 466–471 (2008).
50. Skog, J. *et al.* Glioblastoma microvesicles transport RNA and proteins that promote tumour growth and provide diagnostic biomarkers. *Nat. Cell Biol.* **10**, 1470–1476 (2008).
51. Hong, B. S. *et al.* Colorectal cancer cell-derived microvesicles are enriched in cell cycle-related mRNAs that promote proliferation of endothelial cells. *BMC Genomics* **10**, 556 (2009).
52. Alonso, J. M. *et al.* Genome-wide insertional mutagenesis of *Arabidopsis thaliana*. *Science* **301**, 653–657 (2003).
53. Stein, M. *et al.* *Arabidopsis* PEN3/PDR8, an ATP binding cassette transporter, contributes to nonhost resistance to inappropriate pathogens that enter by direct penetration. *Plant Cell* **18**, 731–746 (2006).
54. Deal, R. B. & Henikoff, S. A simple method for gene expression and chromatin profiling of individual cell types within a tissue. *Dev. Cell* **18**, 1030–1040 (2010).
55. Müller, A. *et al.* AtPIN2 defines a locus of *Arabidopsis* for root gravitropism control. *EMBO J.* **17**, 6903–6911 (1998).
56. Lauber, M. H. *et al.* The *Arabidopsis* KNOLLE protein is a cytokinesis-specific syntaxin. *J. Cell Biol.* **139**, 1485–1493 (1997).
57. Lukowitz, W., Gillmor, C. S. & Scheible, W.-R. Positional cloning in *Arabidopsis*. Why it feels good to have a genome initiative working for you. *Plant Physiol.* **123**, 795–805 (2000).
58. Warming, S., Costantino, N., Court, D. L., Jenkins, N. A. & Copeland, N. G. Simple and highly efficient BAC recombineering using galK selection. *Nucleic Acids Res.* **33**, e36 (2005).
59. Clough, S. J. & Bent, A. F. Floral dip: a simplified method for *Agrobacterium*-mediated transformation of *Arabidopsis thaliana*. *Plant J.* **16**, 735–743 (1998).
60. Gagne, J. M. & Clark, S. E. The *Arabidopsis* stem cell factor POLTERGEIST is membrane localized and phospholipid stimulated. *Plant Cell* **22**, 729–743 (2010).
61. Hellens, R. P., Edwards, E. A., Leyland, N. R., Bean, S. & Mullineaux, P. M. pGreen: a versatile and flexible binary Ti vector for *Agrobacterium*-mediated plant transformation. *Plant Mol. Bio.* **42**, 819–832 (2000).
62. Ikeda, Y., Banno, H., Niu, Q. W., Howell, S. H. & Chua, N. H. The *ENHANCER OF SHOOT REGENERATION 2* gene in *Arabidopsis* regulates *CUP-SHAPED COTYLEDON 1* at the transcriptional level and controls cotyledon development. *Plant Cell Physiol.* **47**, 1443–1456 (2006).
63. Nishimura, T., Yokota, E., Wada, T., Shimmen, T. & Okada, K. An *Arabidopsis* ACT2 dominant-negative mutation, which disturbs F-actin polymerization, reveals its distinctive function in root development. *Plant Cell Physiol.* **44**, 1131–1140 (2003).

Acknowledgements

We are grateful to C. Ambrose, T. Aoyama, F. Berger, D.C. Bergmann, J.R. Ecker, D.W. Ehrhardt, N. Geldner, T. Hashimoto, S. Hennikoff, K. Palme, S. Persson, C.W. Lloyd, A. Sampathkumar, B. Scheres, K. Schumacher, S. Somerville and G.O. Wasteneys for sharing published materials and reagents. We thank the Nottingham *Arabidopsis* Stock Centre for providing seed stocks. This work was supported by Swedish Research Council (Vetenskapsrådet) Grant numbers 2006-522 and 2009-4846, and the Knut & Alice Wallenberg foundation project grant 'ShapeSystems' to M.G., NSF Grant DBI0820755 to J.M.A. and NSF Grant MCB0923727 to J.M.A. and A.N.S.

Author contributions

M.G. conceived the project; M.G. and S.P. designed most of the experiments, S.P. performed the majority of the experiments; S.P., A.G., C.K., Y.I., L.K., P.H. and M.G. designed, performed and analysed experiments apart from recombineering work that was designed, performed and analysed by S.P., A.N.S. and J.M.A. M.G., S.P., A.G., C.K. and L.K. analysed and interpreted the results, A.N.S. and J.M.A. provided unpublished materials, valuable experimental advice, supervised and hosted S.P. during recombineering work. All authors contributed to the interpretation of results. M.G. and S.P. wrote the manuscript. All authors commented on and edited the manuscript.

Additional information

Supplementary Information accompanies this paper at <http://www.nature.com/naturecommunications>

Competing financial interests: The authors declare no competing financial interests.

Reprints and permission information is available online at <http://npg.nature.com/reprintsandpermissions/>

How to cite this article: Pietra, S. *et al.* *Arabidopsis* SABRE and CLASP interact to stabilize cell division plane orientation and planar polarity. *Nat. Commun.* **4**:2779 doi: 10.1038/ncomms3779 (2013).



This work is licensed under a Creative Commons Attribution-NonCommercial-ShareAlike 3.0 Unported License. To view a copy of this license, visit <http://creativecommons.org/licenses/by-nc-sa/3.0/>